Graphene Based Nanocomposites: Synthesis, Characterization and Energy Harvesting Applications

Summan Aman, Maqzia Bashir, Muqaddas Baigum, Muhammad Faizan Nazar, Sajjad Hussain Sumrra, Syed Salman Shafqat, and Muhammad Nadeem Zafar

Abstract Nanotechnology and nanoscience have emerged out as one of the most exciting areas of research today. As an inimitable morphological 2-D carbon material, graphene has triggered a gold rush in the nanomaterial society by introducing controlled functional building blocks. Besides, the mechanical, electrical, and optical properties of graphene make it an attractive contender for applications in solar energy conversion and electrochemical energy devices. Graphene based nanocomposites have been preferred greatly due to their low cost, low density, high electron mobility, exceptional optical transmittance, versatile process ability and excellent thermal conductivity. Subsequently, to encounter the global needs, energy scavenging has become an ultimate part of pervasive sensor network. A gold rush has been prompted all over the world for exploiting the possible applications of graphene-based nanomaterials. The best solution to this problem is to improve the photoconversion efficiencies by optimizing materials and device fabrication.

In this chapter, first of all we have discussed different synthesis methods of graphene nanocomposites like mechanical exfoliation, chemical vapor deposition, liquid phase exfoliation, electrochemical exfoliation and reduction of graphene oxide. For the elucidation of their structural and morphological characteristics, different techniques including SEM, TEM, Energy dispersive X-ray spectroscopy (EDX), UV/Vis absorption spectrum, Raman Spectroscopy, Photoluminescence spectroscopy (PL), X-ray photoelectron spectroscopy (XPS), XRD, Cyclic voltammetry, Impedance spectroscopy, DSC, FTIR and TGA have been discussed. Application potential analysis for graphene-based nanocomposites is discussed based on means including flexible and stretchable electronics, photocatalysis and electrochemical sensing, use in Li-ion batteries, supercapacitors, photovoltaic applications and

S. Aman · M. Bashir · M. Baigum · S. H. Sumrra · M. N. Zafar (✉)
Department of Chemistry, University of Gujrat, Gujrat 50700, Pakistan
e-mail: nadeem.zafar@uog.edu.pk

M. F. Nazar
Department of Chemistry, University of Education Lahore, Multan Campus, Multan, Pakistan

S. S. Shafqat
Department of Chemistry, University of Education, Lahore 54770, Pakistan

A. E. Shalan et al. (eds.), *Advances in Nanocomposite Materials for Environmental and Energy Harvesting Applications*, Engineering Materials,
https://doi.org/10.1007/978-3-030-94319-6_27

hydrogen production. Some of the future concerns have also been discussed related to their feasibility, controlled device fabrication of composites, stability and life span of composite, multistep heterogeneous catalysis and safe dumping of environmental contaminants.

Keywords Graphene based nanocomposites · Energy · Hydrogen production · Solar cells

Abbreviations

PMC	Polymer Matrix Composites
CNTs	Carbon Nanotubes
AFM	Atomic Force Microscopy
CVD	Chemical Vapor Deposition
G-PSS	Graphene [poly (sodium4-styrene sulfonate)]
rGO	Reduced Graphene Oxide
ETOD	3,4-ethylenedioxythiophene
ATRP	Atom transfer radical polymerization
DMF	Dimethyl Formamide
MO	Metal Oxide
NMR	Nuclear Magnetic Resonance
MS	Mass Spectrometry
SEM	Scanning Electron Microscopy
FESEM	Field Emission Scanning Electron Microscopy
LTD	Low Temperature Decomposition
AP	Ammonium perchlorate
XPS	X-ray Photoelectron Spectroscopy
TGA	Thermogravimetric Analysis
CV	Cyclic Voltammetry
PON	Peroxynitrites
MWCNTs	Multi-walled Carbon Nanotubes
AC	Alternating Current
ITO	Indium Tin Oxide
OER	Oxygen Evolution Reactions
NCs	Nanocomposites
GO	Graphene Oxide
STM	Scanning Tunneling Microscopy
NMP	N-methyl pyrrolidone
PSS	[Poly (sodium 4-styrene sulfonate)]
PEDOT	[Poly (3,4-ethlenedioxythiophene)]
APS	Ammonium peroxydisulfate
PFPA	Per fluorophenyl Azide
DMSO	Dimethyl Sulfoxide

PTA	Phosphotungstic Acid
XRD	Powder X-ray Diffraction
FTIR	Fourier Transform Infrared Spectroscopy
TEM	Transmission Electron Microscopy
DSC	Differential Scanning Calorimetry
HTD	High Temperature Decomposition
PSSA	Polyelectrolyte containing aromatic sulfonic acid
ESCA	Electron Spectroscopy of Chemical Analysis
EDX	Energy Dispersive X-ray
GCEs	Glassy Carbon Electrodes
PL	Photoluminescence
PVA	Polyvinyl Alcohol
ECs	Electrochemical Capacitors
LIBs	Lithium-Ion Batteries
ORR	Oxygen Reduction Reactions

1 Introduction

An allotropic carbon having graphene stacks has upraised research in nanotechnology since its discovery. Graphene, a versatile twenty-first century material, is a single-atom-thick structure of sp^2 bonded C-atoms which arrange themselves in a structure like honeycomb, designated as an emerging class of nanomaterials with 2D arranged carbon atoms introducing the building blocks with controlled functionalities [1, 2]. The interfaces thus made contain efficient transport of the electrical energy with having substantial 2D planarity and layers with single atom thickness [3]. The transport of holes and electrons using field effect of electricity having ambipolar nature was allowed by specific characteristics of graphene like zero bandgap along with achievement of the 10^{13} cm^{-2} of carrier concentration and the mobility which can exceed from 15,000 $cm^2V^{-1}s^{-1}$ significantly at the room temperature [4, 5]. According to theoretical calculations, 2630 m^2g^{-1} of surface area is possessed by the graphene along with 200,000 $cm^2V^{-1}s^{-1}$ of mobility at about 1012 cm^{-2} of carrier density with 80–95% of optical transparency having elevated electrical conductivity specifically at the room temperature [6–8]. Graphene contains robust mechanical properties with possession of the Young's modulus having value of 1 TPa along with 42 Nm^{-1} of the breaking strength and outstanding thermal conductivity having value 5000 Wm^{-1} K^{-1} with the fracture strains of ca. 25% which are very favorable for various graphene applications [9]. Due to prevailing environmental problems along with depletion of the fossil fuels in recent years, a great interest has been developed for designing alternative energy sources like devices with energy conversion and storage along with energy densities which can meet this increasing demand. Many properties of graphene like low density, nontoxicity, adjustable process ability and

high mobility of electrons makes the graphene a favorable material for several applications in industry. For the achievement of all these distinctive properties, a possible way is the formation of composite material by the integration of graphene sheets [9]. For example, in the formation of the Ag-nanoparticle films, graphene sheets perform an excellent role on nanoscale ad substrate. Formation of these films which accumulate on nanosheets having a single deposition layer having specific flexibility, forms stable aqueous suspensions [10, 11]. Due to possession of all the mentioned properties of graphene, it can be used for a number of purposes like strain sensors, in packaging industries, in antistatic coatings, electronic devices and as energy storage materials [12, 13]. The minute or the unbroken fibers of PMC (polymer matrix composite) fuse with the polymer matrix in such a way that load can be transferred in-between fibers via matrix. Both the industries and academic area raise significance of graphene-reinforced nanocomposites for study of their thermal and mechanical properties [14]. The special directions and specific geometry possessed by reinforced material can determine mechanical properties presented by nanocomposites [15, 16]. The properties of the nanocomposites like mechanical and electrical strength can be improved by the nanoscale interaction of host material with reinforced material [17]. Recently, researchers have found a considerable difference in special directions of NCs embedded graphene because of the different preparation methods and percentages of graphene in NCs [18]. The appropriate dispersion of the graphene significantly affects its distinctive properties. This issue can be resolved by optimizing materials and introducing controlled fabrication of composites. Consequently, there is a need of graphene having exorbitant qualities for its commercial applications [19]. An appreciating surface-to-volume ratio is possessed by the graphene as compared to the C-nanotubes. Due to presence of this property, graphene became more efficient with ultimate increase in the mechanical strength of composites of graphene with polymers. Graphene also contains the advantage of cost-effectiveness which means that graphene contains significantly low cost than CNTs due to its easy and large quantity availability from the precursors of graphite and from silicon carbide. A brief introduction is aimed to be described in this chapter about the graphene, the preparation methods of graphene nanocomposites followed by the characterization techniques and recent progress in energy harvesting application. At the end, summary and outlook is given to conclude this chapter [20, 21].

2 Synthesis of Graphene-Based Nanocomposites

Graphene was 1st time synthesized in 2004. Many synthesis methods were presented and some of which are given below in Scheme 1.

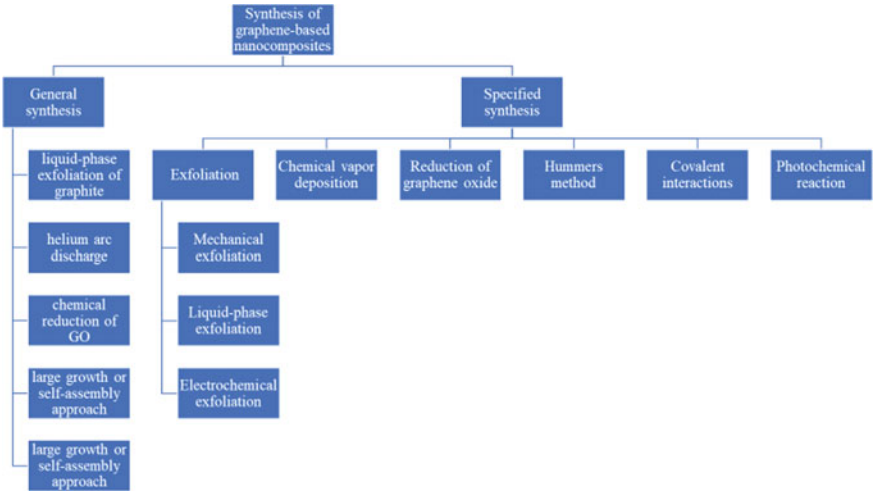

Scheme 1 Synthesis of graphene based nanocomposites

2.1 General Method for the Preparation of Graphene-Based Nanocomposites

As graphene is the fundamental material for synthesis of all functionalities of graphitic material, it faced problems in early research of fullerene and nanotubes [10]. For the utilization of advanced applications of graphene, there is the need for accessibility of the processable nanosheets of graphene in substantial amount. Up to now, two key paths are utilized: large-scale exfoliation and large-scale growth. Some of the techniques like exfoliation of the graphite in liquid phase [22], discharge of Helium arc [23], large scale growth or the self-assembly approach [24], deposition of chemical vapours [25] and the chemical reduction of the graphene oxide [26], have fascinated us to a step closer to the real-world applications for this material.

Among aforementioned approaches for the synthesis of the graphene-based composites, which need the preparation of graphene sheets on a large scale but also ought to be homogeneous distribution. The method of chemical reduction about GO (graphene oxide) appears as very much productive, having low cost and a way to produce mass production for the incorporation of the sheets of graphene into graphene hybrids. As evident from the Fig. 1, the presently focused procedure for the preparation of the graphene-based nanocomposites is by exfoliation of the graphene via combining sonication and oxidation methods accompanied by their reduction using chemical methods [26]. The GO is heavily oxygenated graphene comprising not only carbonyl, epoxy and the OH^- group on the fundamental plane but also the carboxylic group present on the boundary of carbon sheets [28]. The presence of functional groups on graphene oxide act as a presenter site and subsequently make the

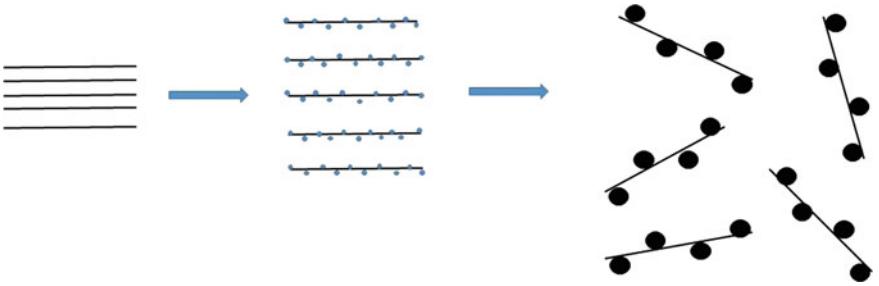

Fig. 1 Schematic route for attachment of nanoparticles on the graphene sheets. (1) Adsorption of metal ions on GO sheets (2) Anchorage of crystalline intercalation and growth of metal nanoparticles on exfoliated GO layers. Reproduced with permission from ref [27]. Copyright 2008, RSC

nanoparticles formed by in-situ synthesis to be embedded on active sites of surface and edges of the graphene oxide sheets. By the conversion of the planar geometry of carbon i.e., sp^2-hybridization to distorted geometry i.e., sp^3-hybridization, GO lost its exceptional electrical conductivity and thus ultimately it becomes electrically insulated [9]. For the recovery of properties of graphene like electrical properties and eliminate functional groups having O_2 for GO for the sake of regeneration of the aromatic graphene network in order to restore the network of graphene which is aromatic and essential.

2.2 Mechanical Exfoliation

The simplest method for the preparation of graphene is considered as mechanical exfoliation [12]. In this preparation method, a graphite piece is mostly used for the purpose of repetitive tape exfoliation which is then moved towards a substrate. Various devices and methods can be used like AFM (atomic force microscopy), Optical microscope, Raman spectroscopy and STM (scanning tunneling microscopy) which is used for the determination of the number of graphene layers. Appreciative quality crystals can be obtained by this preparative technique but have the limitation of only use in prototyping or the lab-scale experiments [29].

2.3 Chemical Vapor Deposition

This technique is helpful in preparing monolayer graphene with large quantity of structural polymers which can be used in several devices. Samples with considerable area can be prepared through exposure of the metals to the precursors of hydrocarbon nature at elevated temperature. It contains several techniques for CVD (chemical vapour deposition) like thermal CVD, plasma-enhanced CVD and the cold or hot

wall CVD etc. The development of the mechanism for the graphene depends on substrate development, which could be initiated by the C-atom growth. Generally observed that due to inertness of graphene to chemicals, it is difficult for the graphene to move from substrate, which results in wrinkles and defects in the material [22]. Chemical vapour deposition has originated as an effective method for production of graphene at large scale. Apart from this, CVD technique is turned out to be practicable technique for large scale fabrication of high-grade graphene [29].

2.4 Liquid-Phase Exfoliation

This method is widely used for graphene fabrication and contains three main steps as; (1) surfactant dispersion, (2) exfoliation (3) purification [30]. Primarily, ultrasound technique was used for exfoliation of the flakes of graphite in suitable solvent like NMP (N-methyl pyrrolidone) [31]. By increasing the time for sonication, we can achieve excessive graphene concentration. By the sonication process, material formed contains thick flakes and we can detach them by applying ultracentrifugation [32]. By increasing speed for centrifugation, we can achieve thinner graphene flakes with small lateral size of the material, mostly non suitable for the composites. In case of dispersion, yield obtained by the relation of graphene flakes for a single layer to total material gives the output of the procedure. Amongst all available variables, two main variables are rotational speed and sonication time. Moreover, the solvents with high reactivity generally increases cost of graphene and also contribute to pollution because graphene contains lower solubility thus uses more of the solvent. However, for purpose of upscaling of fabricated graphene, the most suitable technique is regarded as liquid-phase exfoliation [29].

2.5 Electrochemical Exfoliation

The use of electrical current and the liquid electrolyte comprises of electrochemical exfoliation, eventually utilizes electrodes made up of graphite. This process makes use of oxidation at anode and reduction at cathode for the electrode made up of graphite. For the formation of high-quality conductive layers of graphene, cathodic reaction techniques seemed to be more acceptable and eventually used in the applications like energy harvesting and optics [33]. Compared to pristine monolayer graphene, the material of anode comprises graphene layers in anodic oxidation possessing relatively poor yield and GO in oxidative state [34]. The main reason behind preferring the procedure of electrochemical exfoliation over many other procedures is its capability to yield in one step, easy to perform and requires only a small time of few minutes or few hours for its completion. In contrast, many techniques require a lot of completion time for many non-identical steps. Appropriate factor in nanocomposite development is based on flakes with lateral size, that

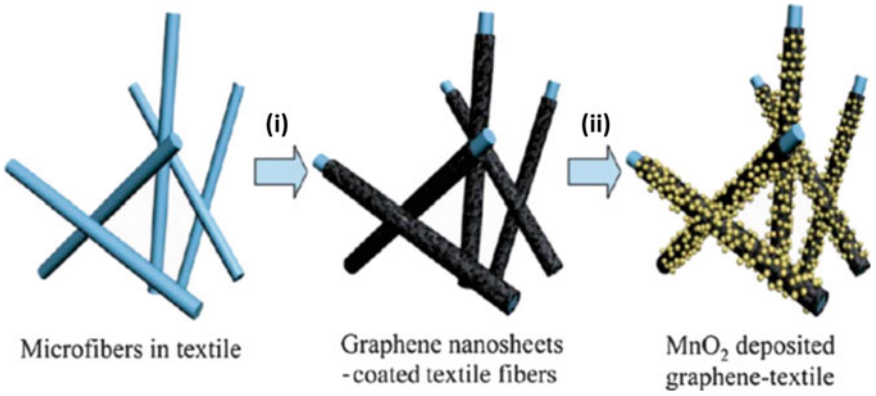

Fig. 2 Electrochemical deposition of MnO_2–graphene nanocomposites (Reproduced with permission from ref [36]. Copyright 2011, ACS)

is directly dependent upon graphite source along with providing exfoliation procedure with intercalation. Likewise, this process is made ecofriendly by using liquid electrolytes [35] (Fig. 2).

2.6 Reduction of Graphene Oxide

Park et al. developed the homogeneous suspension of graphene which was chemically treated in the aqueous media [37]. In this method, initially the graphite dispersion in water is prepared, in which added the aqueous KOH solution. In the opinion of Perk et al. when we treat the KOH which itself is a strong base with the reactive groups like OH, carboxylic acid or epoxy group, it gives a large negative charge on sheets of graphene producing sheets with considerable coating of positive and negative ions. For the stabilization of the potassium oxide modified GO for a long time, hydrazine monohydrate solution is added into it. It ultimately results in the development of the homogeneous suspension of above solution i.e., Hydrazine-potassium hydroxide modified GO, making it stable for about 4 months [38]. For Instance, G-PSS [Graphene poly(sodium 4-styrenesulfonate)] was initially produced by the reduction of aqueous suspension containing graphene oxide along with the hydrazine monohydrate present accompanied with polyelectrolyte of PSS. Performing this procedure, PSS [poly(sodium 4-styrenesulfonate)] was adsorbed onto rGO surface (Reduced Graphene Oxides) via noncovalent interactions of π–π bonds joining the rGO sheets at basal planes and the aromatic rings [39, 40]. PSS is called an ionic stabilizer in reactions containing rGO because it contains negatively charged ions like -SO_3- and produces homogeneous rGO suspensions in aqueous media. Afterwards, there is the formation of the hybrid materials of the G-PSS: PEDOT (Graphene [poly(sodium 4-styrenesulfonate)]: [poly(3,4-ethylenedioxythiophene)])

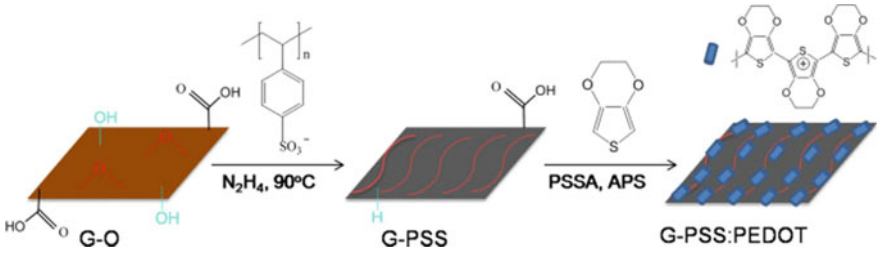

Fig. 3 Schematic formation of G-PSS: PEDOT nanocomposites (Reproduced with permission from [41]. Copyright 2011, SCI)

by the in-situ polymerization of the ETOD (3,4-ethylenedioxythiophene) along with APS (ammonium peroxydisulphate) in the presence of G-PSS. The rGO plates coated with PSS can function as the template in polymerization reactions to connect growing chains of PEDOT [poly(3,4-ethylenedioxythiophene)] on the G-PSS surface. The resulting material formed is hybrid nanomaterial of G-PSS: PEDOT (Fig. 3).

2.7 Hummers Method

Modified Hummers method was employed for the synthesis of the nanocomposites of the Ni/Graphene from the GO-precursors. GO-gel and the Ni(II)acetate tetrahydrate were used as the starting material in a ratio of Ni:C as 5%:95% of atomic ratio. For this purpose, adequate amount of Ni-acetate was dispersed in water followed by mixing with GO-gel. The mixture was changed to the dark brown shade before ultrasonification which was stirred slightly to get homogenized solution and then ultrasonicated at 25 °C for about 10 min. By adding 1 M NaOH solution, 10–12 pH was maintained for mixture while stirring. Prior to place the mixture was heated for 60 min at 70 °C in a closed container, solution was stirred again for 10 min. Gradually, heating was increased within next 60 min up to 95 °C.

Afterwards, centrifugation of the uniform solution was done and by double distilled water remaining contaminants were repeatedly rinsed and again centrifuged. Resultantly, the obtained precipitates were dried in vacuum to get precursor powder of Ni-hydroxide and graphene. Finally, by hydrothermal treatment for 3 h at 350 °C, the above nanocomposites were reduced to nanocomposites of Ni/graphene [42].

2.8 Covalent Interactions

The other suitable method for the fabrication of the nanocomposites of graphene is by covalent reaction. Covalent bonding of GO and graphene to the surface is done by using click chemistry, ATRP (atom transfer radical polymerization) amide

bonding or the diazonium salts [43]. Ionic liquids, per fluorophenylazide (PFPA), polymer, organic nitride, azidotrimethylsilane, p-phenyl-SO_3H, porphyrin as well as the nanoparticles can covalently bind to the graphene [44, 45]. The bonding present between the graphene sheets having covalent functionalities is amide bonding [46].

Stankovich et al. presented incorporation of GO with the isocyanate having organic nature by formation of esters of carbamate and amide with OH and carboxyl group on GO-surface [43]. Through amide bonding, the porphyrin ring of (aminophenyl)-10,15,20-triphenyl porphyrin containing amine functionality were also bonded covalently to the GO in DMF (dimethyl formamide) (Fig. 4a) [44]. Similarly, ionic liquids terminated at amine were made to attach at the graphene for polydisperse nanocomposite formation that can easily disperse in aqueous media, DMSO (dimethyl sulfoxide) and DMF for more than 3 months because of the presence of electrostatic forces in between different units of ionic liquid on the surface of graphene [45]. In other works, the amide bonding along with chemical reduction was used for the fabrication of the alkylated graphene papers via alkylation of GO [46]. Thus, produces the eternally conductive papers of alkylated graphene containing ordered structures having applications in supercapacitors, catalysis, Li-ion batteries and biocompatible materials.

Another way of covalent reaction is utilization of the diazonium salt for preparation of the graphene-based nanocomposites. In another research work, there occurs the sulfonation of the partially-reduced GO by aryl-diazonium salt that produces SO_3H group (sulfonated group) on sheets of graphene having S to C ratio of about 1:35. Moreover, the reduction of this sulfonated GO was done by hydrazine for removal of most of the surplus functional groups containing oxygen. The solubility of sulfonated graphene is about 2 $mgmL^{-1}$ at the pH of 3–10 [48]. Similarly, for the synthesis of the graphene hybrids with bulk of covalent functionalities without any of the oxidized defect, wet chemical method was opted. The intercalation of graphite with K was done in the presence of DME (1,2-dimethoxyethane) solution containing K/Na alloys in accompanied with exfoliation of the single-layer graphene. Due to addition of the diazonium salts, the graphene without oxidation defects was covalently functionalized and it causes no irremediable lattice damage on graphene layers [49]. The attachment of graphene to perfluorophenyl azide (PFPA) using diazonium bonding is due to its thermal and the photochemical activation. As compared to unmodified graphene, sheets of graphene having PFPA functionality were extremely soluble (Fig. 4b) [47]. In this method, the immobilization of the graphene sheet was done on the Si-substrate coupling agent of PFPA-silane, where silane ends get attach to the Si-substrate and PFPA-diazonium to graphene when they are subjected to thermal treatment [50].

For the graphene having covalent functionalities, ATRP (atom transfer radical polymerization) was also significant, starting by the initiator molecule accompanied with polystyrene chain present on the surface of graphene with grafting efficiency of above than 80% [51]. As compared to polystyrene, there is enhanced tensile strength by about 70% and the 57% of Young's modulus for the resulting material which are nanocomposites of polystyrene and graphene containing only the 0.9 wt% of the

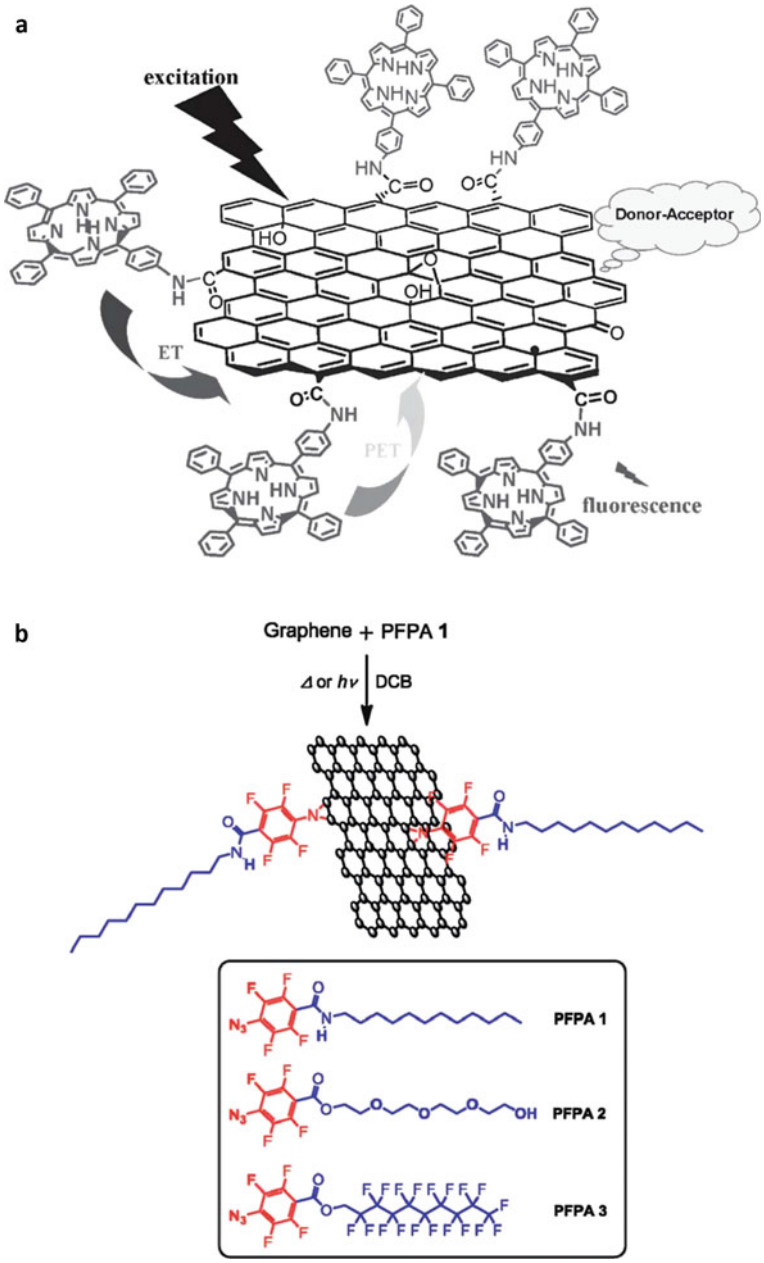

Fig. 4 **a** The hybrids of graphene-porphyrin fabricated through amine covalent bonding. Reproduced with permission from ref [41]. **b** The covalent bonding of graphene and PFTA via diazonium salt (Reproduced with permission from ref [47]. © 2009, John Wiley and Sons (a); © 2010, ACS (b))

graphene sheets. The resultant nanocomposites of polystyrene and graphene have enhanced thermal conductivity as compared to polystyrene by factor 2.6 with the 2 wt% of graphene [52].

2.9 Photochemical Reaction

For the preparation of the nanocomposites of graphene, favourable route is by photochemical reaction [53–56]. Some of the photochemical reactions occur in graphene presence by simple light irradiation resulting in formation of nanocomposites of graphene. For example, the nanocomposites of graphene-TiO_2 can be produced by careful mixing of TiO_2 and GO in ethanol by irradiating UV light in photochemical reactions. The TiO_2 is actually UV-active and when UV-light is irradiated, reduction of GO occurs by the electrons which get excited in the TiO_2 followed by production of nanocomposites of reduced graphene-TiO_2 [57]. Same procedure was adopted for synthesis of nanocomposites of $BiVO_4$- and WO_3-graphene by applying photocatalytic reaction in between GO and precursors. Instead of MO (metal oxide), the deposition of the nanoparticles of metals like Pb, Pt, Au and Ag can be done by the use of radiations [58, 59]. For the reduction of GO to graphene, one approach comprises the fabrication of metals like Pt, Au and Ag nanoparticles on surface of graphene by performing photolysis of PTA (phosphotungstic acid) (Fig. 5) [60]. Meanwhile, the in-situ reduction of metal precursors can be done by PTA which was photolyzed on the surface of graphene. Thus, attachment of metal nanoparticles on graphene surface can be done without using any of the molecular linker. The formation of fine dispersion of nanoparticles of noble metals like Pb, Au and Ag on graphene surface can be done using DMF by two-step photochemical technique. The very 1st step possesses the photochemical reduction of GO to the reduced graphene by using phosphotungstate with irradiation of UV-light. Secondly, formation of composites of graphene-noble metal nanoparticles is done by instant subjecting of metal ions or the compound precursors [53]. Through literature review, it is clear that the photochemical reaction for the production of nanocomposites of silver-reduced graphene can be initiated by the mixing of GO and ammonia-silver complexes using Ag-lamp of 450 W [60]. Similarly, the loading of Ag-NPs was done on GO-using radiations from visible light using photochemical reactions [54]. To prepare GO–Ag nanocomposites, photochemical depositions of Ag NPs on graphene oxide were also developed in an alkaline environment. For the preparation of nanocomposites of GO-Pt using photochemical deposition of the Ag-nanoparticles, photochemical deposition can be used. Pt–graphene nanocomposites were prepared in the same way irrespective of any reducing agent [58, 59].

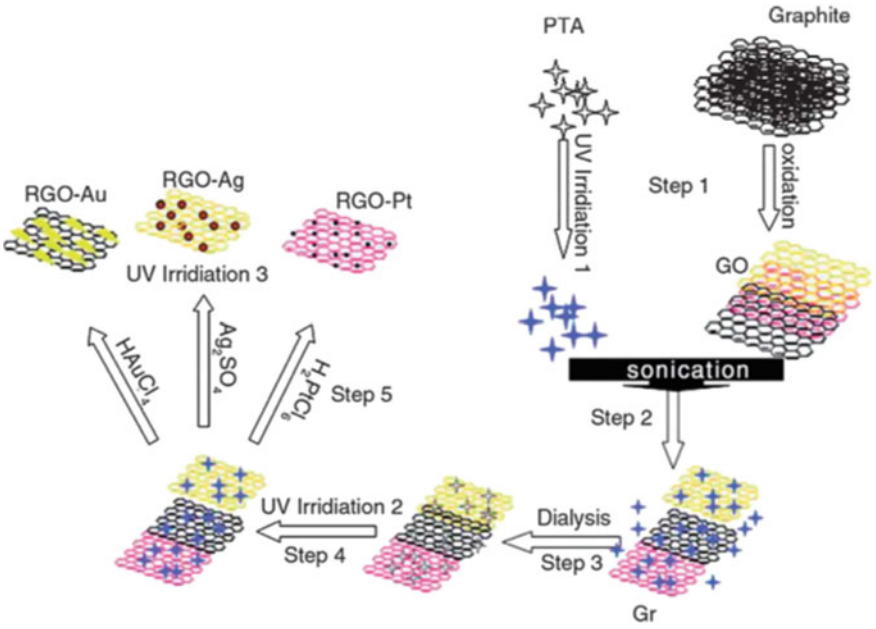

Fig. 5 Photochemical routes to metal NP–graphene nanocomposites (Reproduced with permission fron ref [56]. © 2012, Elsevier)

3 Characterization of Graphene Based Nanocomposites

Nanocomposites are a combination of multilayers of nanomaterial with matrix support of another compound [61]. Hence, their characterization comprises several aspects [62]. The characterization of NPCs based upon analysis of morphological, optical, elemental, structural and functional properties is done by a number of techniques such as NMR, XRD, UV–Visible spectroscopy, MS, FTIR, XPS etc. Optical properties of NCs are recognized by two spectroscopic techniques, namely FTIR and UV–Visible spectroscopy [63].

3.1 TEM and FESEM Images of Silver Nanoparticles on GO-Sheets

SEM (scanning electron microscope) uses the highly focused high-energy beam of electrons for resolution of minor details of the specimen [64]. The signal produced by the interaction of sample and the beam reveals the important details of the sample which also contains information about material orientation, crystalline structure, morphology and the chemical composition of the sample [65]. However, SEM

contains a similar basic principle to light microscopy with the difference that it makes use of an electron beam instead of light. The resolution of SEM is better than a light microscope because of the smaller wavelength of electrons from the light [66]. Hence, SEM have power to reveal minor details of material about its internal structure, commonly as small as of the individual atoms [67].

The images for TEM (transmission electron microscope) and the FESEM (field emission scanning electron microscope) for the nanoparticles of silver on the GO-sheet are shown in figure below. In Fig. 6(a), 2D sheets of the graphene which are almost transparent were fabricated by Ag-particles. The nanosheets of carbon containing a single layer are so thin that it seems to be hard to distinguish them from the Cu-grid supported by carbon. However, edges of carbon sheets and their wrinkled silk waves lead to the conclusion that these particles are actually deposited on the support as given by Fig. 6(b). Instead of this, the Fig. 6(c and d), clearly shows that the synthesized nanoparticles of silver can accumulate on the substrate surface of graphene. Generally, there is presence of functional groups on the edges and planes of the GO. These functional groups (negatively charged) are used for the absorption of

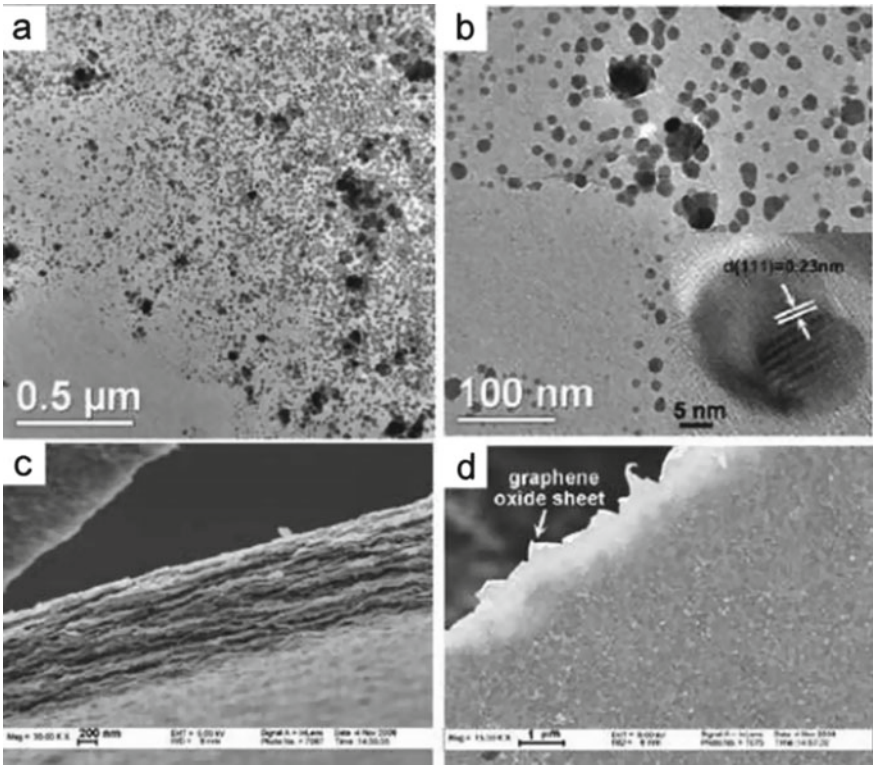

Fig. 6 TEM **a, b** and the FESEM **c, d** images for the deposited silver particles on the surface of GO-sheets (Reproduced with permission from ref [69]. © 2009, Wiley InterScience)

nanoparticles and inorganic materials on graphene surfaces. Thus, positively charged ions can easily interact with negative functionalities by using electrostatic interactions. In-situ reduction of ions using glucose permits the adsorption of nanoparticles of silver on GO-sheets. By applying this method, some nanoparticles get deposited on the GO-sheet surface and some on their edges [68].

It is clear from experiments that we can process aqueous solution of graphene-based sheets into the films and the paper like material [9, 26]. The sheets of GO coater with silver can easily be incorporated to form macroscopic film by drying it on substrate which contains a shiny luster of metal which shows mirror-like characteristics. But the film containing discrete GO-sheets contain very poor reflectivity. It is generally assumed that the origin of Ag-mirror films is due to assembly of Ag-nanoparticles on the substrate surface [70]. This system contains the formation of macroscopic films containing mirror-like appearance and can be characterized by restacking on nanoparticle film by silver (Fig. 6c).

3.2 TEM and FESEM Images of GO-Co_3O_4 Nanocomposites

From Fig. 7, SEM images of synthesized nanocomposite reveals that exfoliated sheets of GO were arbitrarily decorated by the particles of 100 nm size which are spherical in shape [27]. These nanoparticles formed by in-situ method result in the exfoliation of layered GO. In Fig. 8 the TEM images of the nanocomposites of GO-Co_3O_4 seemed to be brighter than those surrounded by thin film. This can be clearly seen that sheets of GO contain functional groups on it's both sides including epoxy and OH group by which Co_3O_4 can easily get attached to the support [68].

3.3 Differential Scanning Calorimetry (DSC)

DSC (differential scanning calorimetry) is an electroanalytical technique which measures the heat flow across the system as a function of time or temperature when we expose the sample to controlled and programmed temperature. In this technique, we limit the specific heat capacity of pure compounds or mixtures and determine the catalytic effect of materials. Differential scanning calorimetry was conducted for the measurement of the catalytic effect produced by the nanocomposites of GO-Co_3O_4 produced by their thermal decomposition on ammonium perchlorate. Figure 9 shows the curve for DSC that contains decomposition of the AP (ammonium perchlorate) along with AP and GO, Co_3O_4 and the GO-Co_3O_4 nanocomposite [27]. Usually, the thermal decomposition of the ammonium perchlorate occurs in 3-main steps: (i) phase transition of the material at 240 °C for endothermic reaction, (ii) decomposition at low temperature of about 316 °C i.e., LTD (low temperature decomposition) and (iii) decomposition at high temperature of about 460 °C i.e., HTD (high

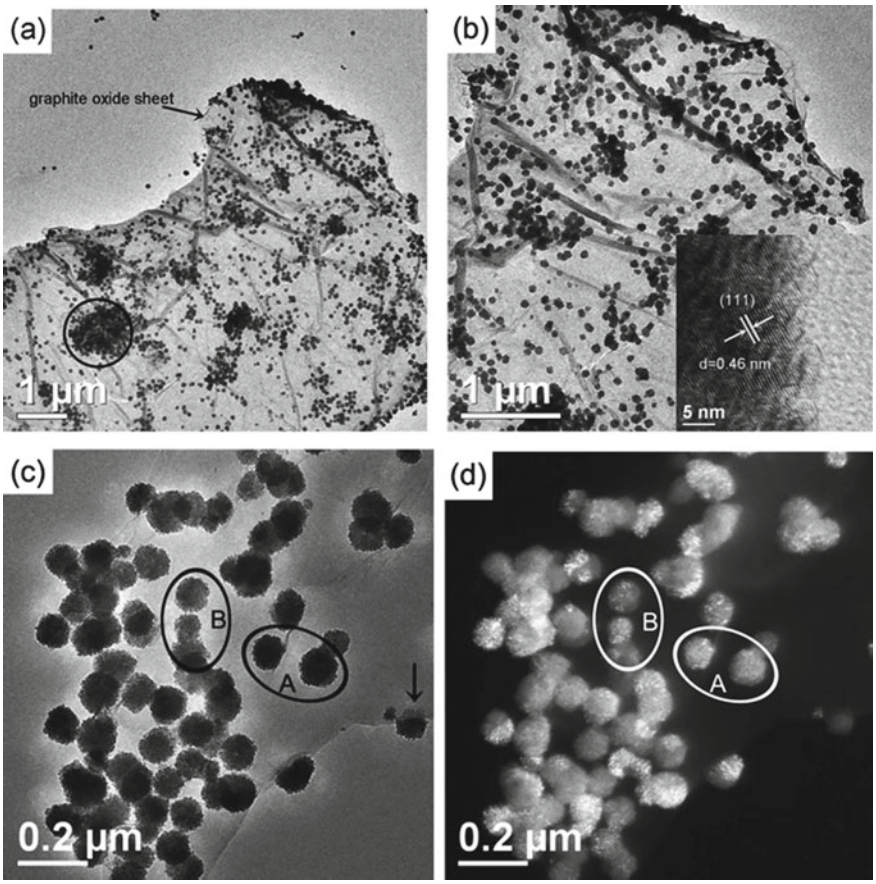

Fig. 7 FESEM images of GO-Co_3O_4 nanocomposites (Reproduced with permission from ref [27]. © 2008, RSC)

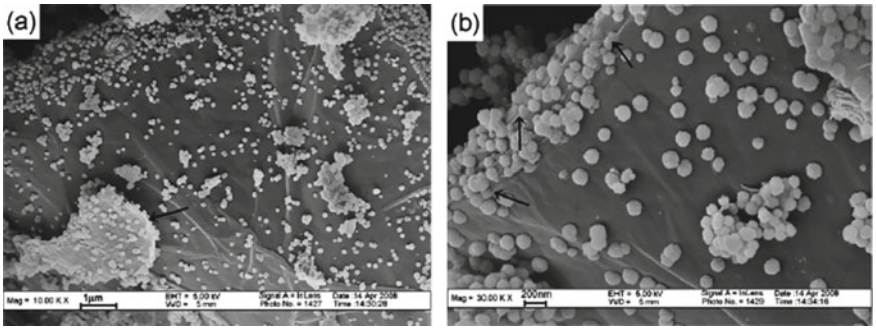

Fig. 8 TEM images of GO-Co_3O_4 nanocomposites (Reproduced with permission from ref [27]. ©2008, RSC)

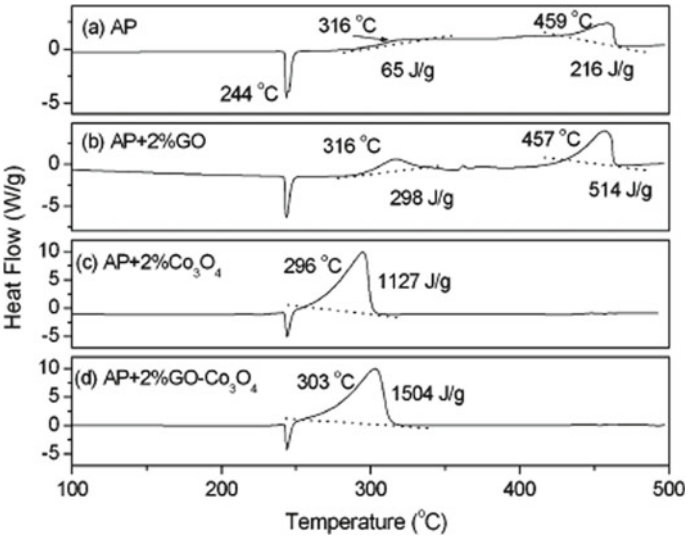

Fig. 9 Curves for DSC showing decomposition of the AP, AP with 2% GO, AP with 2%Co_3O_4 and the AP with nanocomposites of 2% Co_3O_4-GO (Reproduced with permission from ref [27]. © 2008, RSC)

temperature decomposition). It is very critical to decrease decomposition temperature and increase endothermic heat for industrial applications of the AP. Two apparent exothermic peaks for AP can be observed when graphene was added in it, accompanying the new single peak of exothermic current at about 360 °C and it was observed that heat of these exothermic steps is more than AP [68]. This effect could be observed due to the catalytic nature of the GO. The introduction of the GO-Co_3O_4 and Co_3O_4 can reduce the temperature of the LTD and HTD and combine these steps into a single step. Decomposition temperature of 2% GO-Co_3O_4 (303 °C) and AP along with 2% Co_3O_4 producing exothermic reactions are nearly close to each other with quantities of 1504 and 1127% respectively. Therefore, for catalytic decomposition of AP due to cumulative effect of all distinct components, by adding GO-Co_3O_4 only decomposition is not increased but also resulted in an increase in the exothermic heat for AP, resulting in excellent catalytic properties of AP [27].

3.4 X-Ray Diffraction Analysis (XRD)

The crystal structure of a material can be best identified by using XRD along with interlayer distance of GO and graphene and its composition. XRD is based upon Bragg's law [71]. Figure 10(a) shows the XRD pattern for the GO, graphite and graphene. While the Fig. 10(b) represents composite of Ni and graphene before and after its reduction along with metallic Ni. Figure 10(a) shows that graphite contains

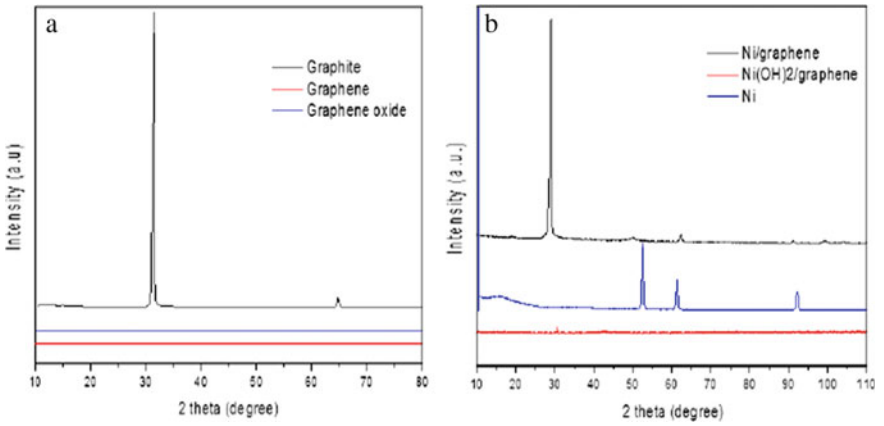

Fig. 10 (a) XRD specta for graphite (black), GO (blue) and the graphene (red). (**b**) Ni (blue), Ni/graphene nanocomposite (black) and the $Ni(OH)_2$ precursor (red). (Reproduced with permission from ref [72]. © IOP Publishing Ltd)

diffraction peaks which are very sharp and contain high intensity at about $2\theta = 31°$. We obtain (002) orientation with d-spacing of 0.33 nm. The peak for graphite disappears after oxidation and is proven by the appearance of blue and red lines for GO and graphene respectively. As evident from Fig. 10(b) after thermal reduction of hydrogen, the peak for $Ni(OH)_2$ disappears proving the reduction of $Ni(OH)_2$ into elemental Ni in formation of Ni/graphene composite. And there is an appearance of three-different peaks in its diffraction pattern i.e., at about $2\theta = 52.8$, 61 and the 93° corresponding to the reduction of Ni in Ni/graphene composite. Thus, these results clearly indicate that Ni gets reduced on graphene surface [72].

3.5 Raman Spectroscopy

Raman spectroscopy is a type of molecular spectroscopy which contains the interaction between light and matter for better investigation of material's characteristics. Information is gained by scattering of light. As it identifies the vibrational modes of interatomic bonding along with structure produced because of differences in structural features of molecules. This technique utilizes a monochromatic laser for interaction of phonons with molecular-vibration mode, resulting in movement of energy up and down in different energy levels by the inelastic scattering [73]. So, in order to elucidate the electronic distribution, Raman spectroscopy was performed. D and G bands are shown in spectra for characterization of graphene. G contains atoms with sp^2-hybridization along with plane vibrational modes while D with sp^3-hybridization show bands as defected bands. Figure 11 shows D and G bands which are present at 1578 cm^{-1} and 1658 cm^{-1} respectively. It has been observed that no shift produced in

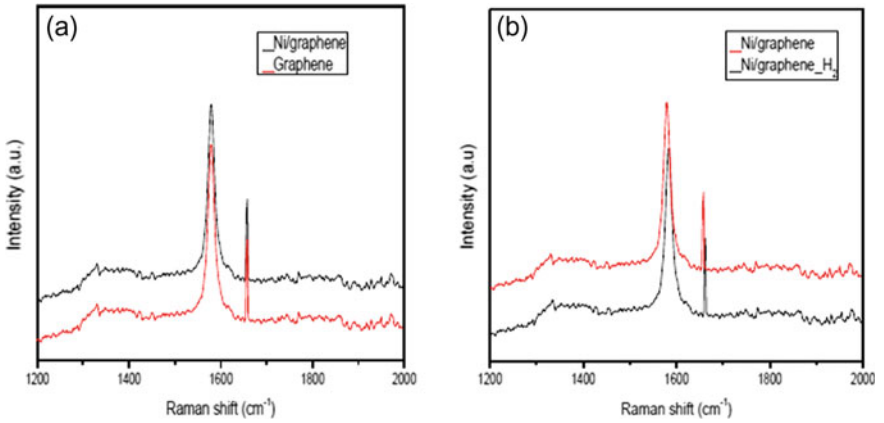

Fig. 11 Raman spectra of graphene, Ni/graphene, and Ni/graphene_H_2 (Reproduced with permission from ref [72]. © IOP Publishing Ltd)

position of peak for Ni/graphene while when it gets charged with hydrogen it contains a peak. From their spectra, it is clear from D/G ratio that sp^2-hybridization is strengthened while sp^3 is weakened. As the number of graphene sheets increases, there is an increase in high-frequency peaks due to their proportionality to number of vibrational modes. Hence, graphene platelet packing gives peaks with low intensity [72]. The shift in D-peaks of spectra can be observed due to restacking of platelets of graphene when Ni/graphene gets charged with hydrogen.

3.6 Fourier Transform Infrared Spectroscopy

FTIR spectroscopy is the technique employed to recognize vibrational modes in the molecules [74]. It is also known as vibrational spectroscopy. Comparison of FTIR spectra for nanocomposites of GO, G-PSS and the G-PSS: PEDOT is given in Fig. 12(a). Spectra for GO contains C = C peak at 1625 cm^{-1} while peaks for O-based functionalities like C = O, C-O (epoxide or ether), carboxy C-O and alkoxy C-O are present at 1730, 1410, 1230 and 1050 cm^{-1} respectively [75, 76]. A comparison of GO and G-PSS spectra exhibits a decrease in stretch intensities for C-O and C = O which suggest the reduction of RG-O (reduced graphene oxide) platelets. Furthermore, new bonds describing PSS polyelectrolyte appear at 1180 and 1088 cm^{-1}, showing introduction of PSS on RG-O surface. Peaks for G-PSS: PEDOT in FTIR spectra are present as; C = C at 1524, C–C at 1320, S–O at 920 and C-S at 680 cm^{-1} produced in PEDOT by thiophene ring, while peaks containing value of 1088 and 980 cm^{-1} represent the S = O stretching vibrations present in SO_3-group [41]. Results predict the formation of PEDOT in the form of composites and in the form of association with the G-PSS [75].

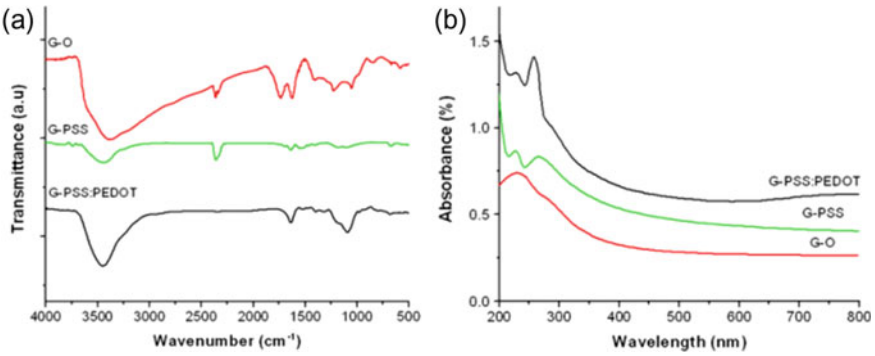

Fig. 12 **a** FTIR spectra for GO, G-PSS and G-PSS: PEDOT composite. **b** UV–Vis spectra for these composites (Reproduced with permission from ref [41]. © 2011, SCI)

Dispersions of above-mentioned composites in aqueous media were confirmed by UV–Vis spectra as given in Fig. 12b. Characteristic peak for GO in UV–Vis spectra was given at 232 nm and peak at 300 nm represents π–π∗ transition in aromatic carbons and the n–π∗ transition to C = O respectively. Two peaks at 226 and the 268 nm are given in spectra for G-PSS which were originally allocated to PSS-polyelectrolyte [77, 78] and the π–π∗ transition RG-O contain red-shift from GO. For composite of G-PSS: PEDOT, peak at 275 nm due to PSSA (polyelectrolyte containing aromatic sulfonic acid) arises its broad absorption peak at 750 nm [79].

3.7 X-Ray Photoelectron Spectroscopy (XPS)

XPS (X-ray photoelectron spectroscopy) was commonly used to study surface characteristics along with analysis of biomedical polymers. This can also be called ESCA technique i.e., the Electron Spectroscopy of Chemical Analysis and employed for study of elements with mass ranging from 10–200, which are stable in vacuum conditions or made stable by just cooling the molecule. Moreover, it is not suitable for H_2 and He. This is regarded as the most informative surface technique providing other applications like most quantitative information about chemical information and readily interpretable technique as compared to other techniques [80]. For monitoring composition of graphene oxide, G-PSS and composites of GPSS: PEDOT, XPS was performed (Fig. 13) [41]. The XPS spectra for the GO can be divided into four-main parts showing C-atoms present in different O-containing functionalities i.e., C in C-O (286.6 eV), C = O (287.9 eV), non-oxygenated C (284.8 eV) and O-C = O (289.2 eV) [81, 82]. 1s C spectra for composites of G-PSS: PEDOT is given in Fig. 14. Same O-functionalities are present in both GO as well as G-PSS: PEDOT but contribution of oxygenated carbon is much less proving that many O-based functionalities are removed during reduction. Moreover, two supplementary peaks at about

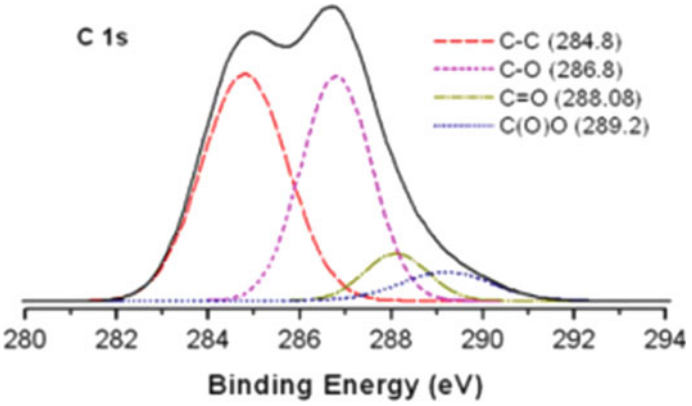

Fig. 13 C 1s XPS spectrum of G-O (Reproduced with permission from ref [41]. © 2011, SCI)

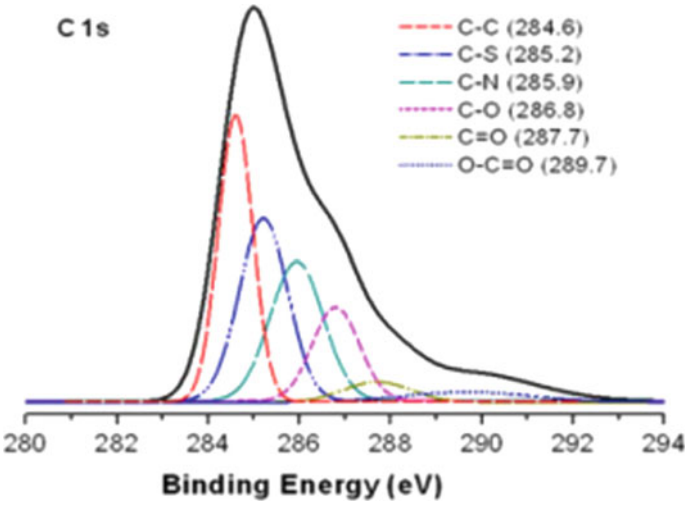

Fig. 14 C 1s XPS spectra of G-PSS: PEDOT composite (Reproduced with permission from ref [41]. © 2011, SCI)

285.2 eV and 285.9 eV are seen which are due to C-S in PSS as well as C-N in hydrazine respectively [82]. Hence, the PEDOT formation was confirmed by 2p S spectra (Fig. 15). Spin-split duplets show peaks for binding energy at 164.2 eV and 165.5 eV in case of S-atoms present in PEDOT, peak due to sulfonic acid (SO_3-H^+) group arise at 168.6 eV [41].

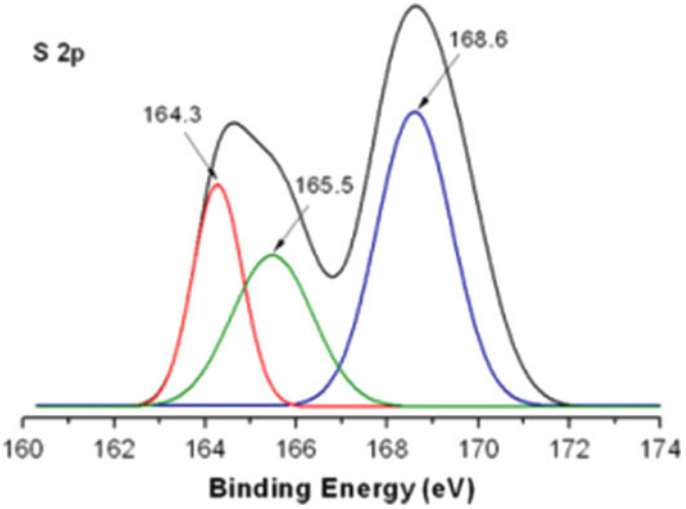

Fig. 15 S 2p XPS spectra of G-PSS: PEDOT composite (Reproduced with permission from ref [41]. © 2011, SCI)

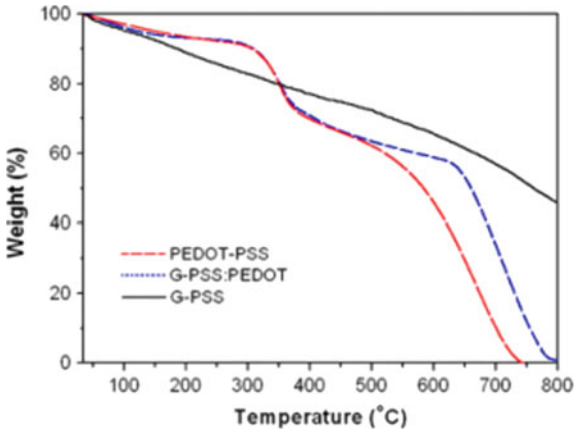

Fig. 16 TGA spectra of G-PSS, PEDOT: PSS and G-PSS: PEDOT composites obtained at a heating rate of 10 °C min^{-1} under nitrogen (Reproduced with permission from ref [41]. © 2011, SCI)

3.8 Thermogravimetric Analysis

TGA (thermogravimetric analysis) is a type of analysis which contains the measurement of the mass of the given substance over time when the sample is subjected to temperature and atmospheric changes. Consequently, information such as phase transitions, absorption, desorption, adsorption as well as thermal stability is determined. Hence, the thermal stability for the G-PSS: PEDOT hybrids was determined. The TGA data for the G-PSS: PEDOT, PEDOT: PSS and the G-PSS are given in Fig. 16. Both of the above samples contain good thermal stability only up to around 315 °C

which is 1st decomposition temperature employed, which also can be employed to the PSS decomposition. Whereas, PEDOT: PSS exhibits a relatively low temperature of 575 °C whereas G-PSS: PEDOT contains the enhanced thermal stability and shows 645 °C of 2nd decomposition temperature employed. Thus, it is clear that thermal stability of G-PSS; PEDOT is higher than PEDOT; PSS, which is due to effective hybridization present between RGO and PEDOT [41].

3.9 Energy Dispersive X-Ray (EDX)

The EDX (energy dispersive x-ray) spectroscopy which is also called EDAX or EDS analysis is actually x-ray technique which is used for the identification of elemental composition of given material. The peaks obtained give identification of each of the individual component of material in its true composition. Consequently, the analysis performed for the GO-MnO_2/hemin and a comparison were done with GO and the rGO/hemin when analyzed under same conditions. The ratio of relative atomic weight for many different samples is given in Table 1 [83].

In terms of iron and manganese peaks, difference in EDX spectra for rGO/hemin and the GO-MnO_2/hemin is shown in Fig. 17. The appearance of a new Mn peak for GO-MnO_2/hemin was expected which was absent in case of rGO/hemin and is in accordance with formation of nanocomposites of GO-MnO_2/hemin as shown in Fig. 17. Similarly, there has been an increase in atomic weight from 1.75 to 2.87 for Fe in rGO/hemin and GO-MnO_2/hemin respectively. The nanoneedle growth of MnO_2 with proper orientation was supported by Mn oxidation in the water-isopropanol system. It was assumed that this process causes exfoliation of sheets of GO [84]. Exfoliation of GO driven by the MnO_2 allows more interaction of hemin with graphene sheets for the formation of GO-MnO_2/hemin, which describes the increase in peaks of Fe in EDX spectra for nanocomposite material [83].

Table 1 %age weightage of the GO for EDX analysis along with GO after its treatment with the hemin for the formation of rGO/hemin and GO-MnO_2/hemin formed by treatment of GO-MnO_2 with hemin (Reproduced with permission from [83]. © 2018, ECS)

Atomic weight percentage (%)	GO	rGO/hemin	GO-MnO_2/hemin
C	68.13	70.78	30.40
O	31.70	25.32	41.73
Cl	–	2.15	0.59
Fe	–	1.75	2.87
Mn	–	–	24.41

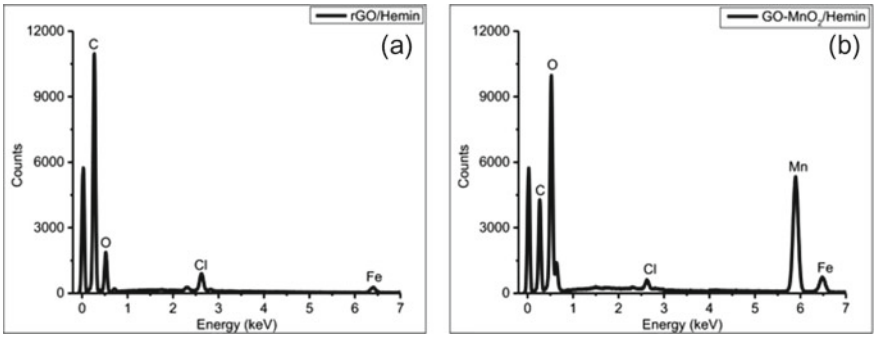

Fig. 17 EDX spectra for the nanocomposites of GO **a** EDX spectra for the rGO/hemin **b** EDX spectra for the GO-MnO_2/hemin (Reproduced with permission from ref [83]. © 2018, ECS)

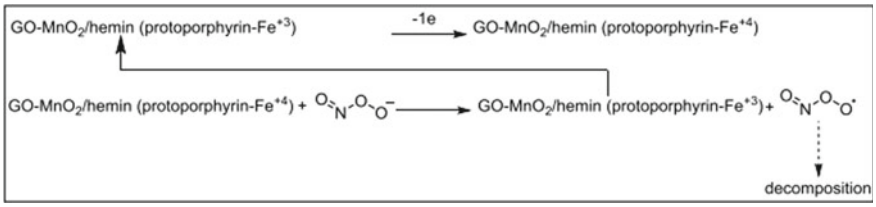

Fig. 18 The proposed mechanism for catalytic oxidation of the PON on the nanocomposites of GO-MnO_2/hemin using GCE interface (Reproduced with permission from ref [83]. © 2018, ECS)

3.10 Cyclic Voltammetry (CV)

Cyclic voltammetry is considered to be the influential technique which is used for investigation of oxidation and reduction processes occurring within the molecular species. The plot of CV is called voltammogram. Graphically, applied potential is shown on x-axis and resulting current on y-axis. CV data can be reported by two conversions i.e., oxidation and reduction [85]. So, electrochemical performance for the modified GCEs by GO-MnO_2/hemin and the rGO/hemin (glassy carbon electrodes) were determined at the same time using phosphate buffers. Now the suspensions for both of the above species with brown–red and brown-black color were deposited on the GCEs (glassy carbon electrodes) which were freshly polished and set them to dry before use. Typical response of these species for volumetric measurements in the presence and absence of the PON (peroxynitrite) was given in Fig. 18. In the phosphate buffer at 7.4 pH the solutions of PON made by 1 μM of SIN-1 stock solution were used. In presence of PON the oxidation peak or rGO/hemin was seen at +1.1 V which indicates catalytic oxidation of the PON supported by hemin present on graphene, the mechanism of which is reported in literature [86, 87]. GO-MnO_2/hemin contain a similar mechanism which is given in Fig. 18 [83].

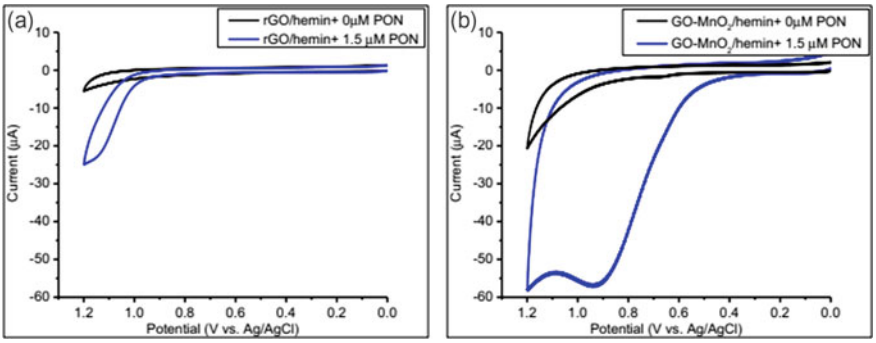

Fig. 19 CV of the GCEs which are modified by GO-MnO_2/hemin and rGO/hemin in the presence and absence of PON prepared by the stock solution of SIN-1 with 1 μM concentration and 7.4 pH. scan rate used for all the voltammograms was 0.1 v/s: **a** voltammetric response of the rGO/hemin in the presence and absence of PON of 1.5 μM **b** voltammetric response of GO-MnO_2/hemin in the presence and absense of PON of 1.5 μM (Reproduced with permission from ref [83]. © 2018, ECS)

In graphene/hemin composite, the integration of MnO_2 transfer the peak for catalytic oxidation of PON toward lower potential of about 200 mV. Therefore, a pronounced peak appears at +0.9 V for catalytic oxidation of PON versus Ag/AgCl as given in Fig. 19. The shift towards the lower positive potential in catalytic peak for MnO_2 shows that incorporation of MnO_2 with GO/hemin helps in lowering the barrier for the electrochemical oxidation of the PON on modified interfaces. Likewise, exfoliation of the graphene oxide supported by nanoparticles of MnO_2 support more incorporation of hemin catalyst with the nanocomposite material. When lower positive potential is applied, results in pronounced response of current [83].

3.11 Amperometric Measurements

Amperometry measurements include application of oxidizing and reducing potential to working electrode with consequent measurement of faradic current produced. During the measurement, optimized value of current and potential is made fixed even with variation of function of the time [88]. For the comparison of electrolytic activity of different materials, amperometric measurement are performed. For this purpose, the aliquot of PON prepared by stock solution oh SIN-1 of 1 μM concentration was used. Thus, amperometric measurements were done for the PON modified electrodes along with comparison of rGO/hemin and GO-MnO_2/hemin after every injection for the sensors. Applied potential in both cases was +1 V. Figure 20 represents the response of induced current when PON aliquot was added to the electrochemical cell in the 7.4 pH phosphate buffer. A remarkable large response for the production of current by catalytic oxidation of PON was seen in CV measurements for GO-MnO_2/hemin as compared to rGO/hemin. There occurs a linear response between

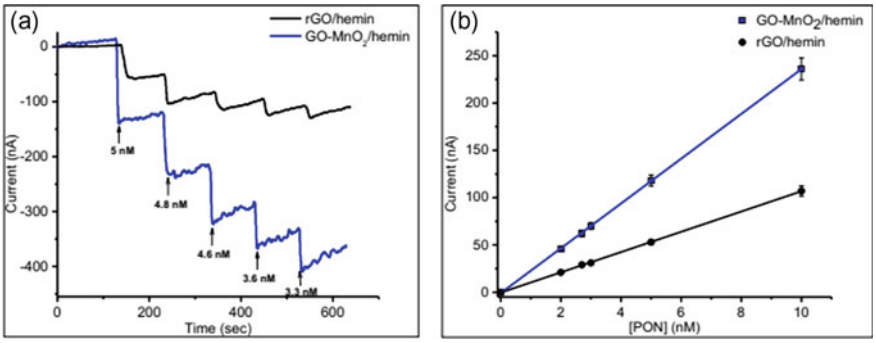

Fig. 20 Representative amperometric responses (nA) (Reproduced with permission from ref [83]. © 2018, ECS)

the added PON and measured current in amperometric measurements in 2.0–10.0 nM range (Fig. 20). Sensitivity of about 23.7 nA/nM in case of GO-MnO_2/hemin was analyzed in contrast with rGO/hemin of ~10 nA/nM. Relative detection limit for good stability of sensors with use of GO-MnO_2/hemin was 2.0 nM [83].

3.12 Photoluminescence Spectroscopy

The photoluminescence spectroscopy is the type of non-destructive spectroscopic technique for investigation of electronic structure for specified material. In this method, we expose light to the sample which absorbs the incident light and transfer excess light for excitation within the material that leads to photoluminescence. Therefore, PL (photoluminescence) spectrum of MWCNTs (multi-walled carbon nanotubes) for the excitation at about 325 nm and account for its structured band at 447 nm. p-p* transitions resulted from excitation of electrons of MWCNT from lower energy state to higher energy state as illustrated by the PL spectrum shown in Fig. 21. Eventually, recombination of the electron–hole at band edge for sp^2 clusters can be demonstrated by blue fluorescence obtained at shorter wavelengths having small band gap [89]. Band gap for the semiconductors of CNT was 1eV by which we can elucidate their structure at about 447 nm. When PVA (polyvinyl alcohol) is added to the MWCNT, fluorescence improvement was observed [90].

3.13 AC Impedance Spectroscopy

AC (alternating current) impedance spectroscopy is an electrical measurement technique used as a rapid, non-destructive tool for characterizing composite microstructure. It measures the properties of material like resistance and capacitance by applying

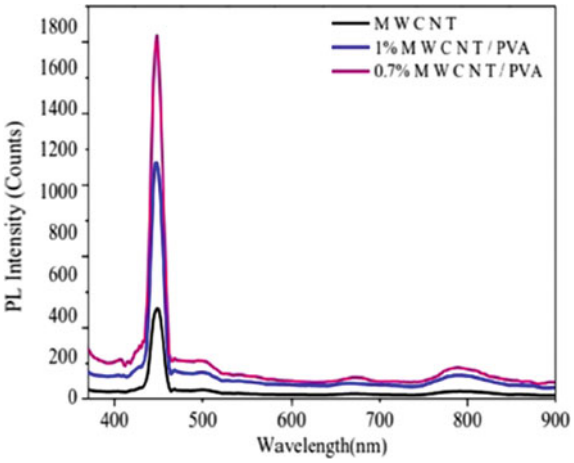

Fig. 21 PL Spectra of MWCNTs/PVA nanocomposites (Reproduced with permission from ref [90]. © 2016, Elsevier)

excitation signal for sinusoidal AC and is widely used in combination with engineered phage for sensing applications [91]. For the explanation of different properties of n-ZnO and reduced graphene oxide incorporated n-ZnO like gas sensing, AC impedance spectroscopy was performed. Both the rGO and the nZnO contain the analyte gas trapping ability and thus contribute to change in conducting properties [92]. Figure 22 illustrates imaginary parts for the impedance of n-ZnO/rGO for their exposure to air as well as different H_2S concentrations at 90 °C. The relaxation frequencies can also be indicated for ZnO/rGO-5 through this figure which can be evaluated by plotting impedance versus frequency (logarithmic frequency) [93]. When H_2S is employed, there is an observed decrease in the imaginary part of Im-(ZnO). With increase of H_2S concentration, additional electron flow was observed with decrease in barrier height. The shifting of peaks towards large frequency range can be related to easy flow of the charge carriers by using AC current [94–96].

4 Energy Harvesting Applications

The principle behind energy harvesting is all about the available environmental energy and its conversion to operable electrical energy. This energy is either used directly, collected or stored in the areas with no any grid power or the use of solar panels or wind turbines if inconvenient. To meet worldwide challenges, applications of energy harvesting have been playing an important part of universal sensor network. Because of the extraordinary application of graphene like low cost, non-toxicity and high flexibility, these are used as promising electrode for use in energy harvesting appliances. These devices are used for applications like self-powering biomedical

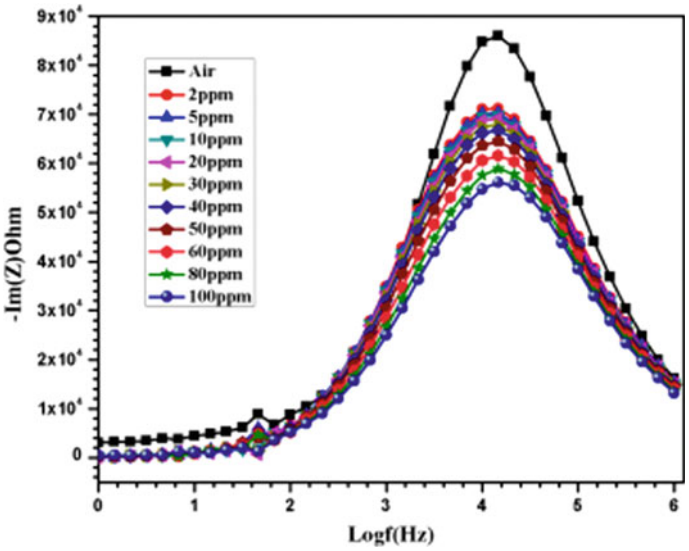

Fig. 22 Imaginary part of impedance for the n-ZnO/rGO-5 when exposed to the air along with H_2S gas with 2–100 ppm concentration at 90 °C (Reproduced with permission from ref [93]. © 2019, ACS)

sensors, portable electronic devices and sustainable environmental monitors, because of their ability to build a battery with long lifetime and development of a self-powered system [97].

4.1 Graphene-Based Flexible Logic Devices

In electronics, the promising applications of graphene are because of their large surface area of about 2630 m^2g^{-1} along with capacity to accelerate transfer of holes and electrons along their 2D (2-dimensional) surface. Therefore, there is great importance of research for energy harvesting applications. An important example is nanogenerator which is used for conversion of mechanical energy into electrical energy. Logic devices which are flexible and stretchable, can maintain the apparent applications of bio-integrated and wearable electronics. Many efforts are being done for the development of such devices containing electrode materials which are oxide based, CNTs or polymer based [97–99]. However, even now after many years of intensive work, there are several challenges present regarding to the inherent electrical or mechanical weaknesses which are increasing problems due to its closeness to current fabrication technology. However, graphene also offers magnificent value for Young's modulus because of strong bonding of atoms along with mechanical flexibility, providing superlative electrical properties [100]. The electronic devices which contain stretchability, flexibility and conformal properties are best fit for this

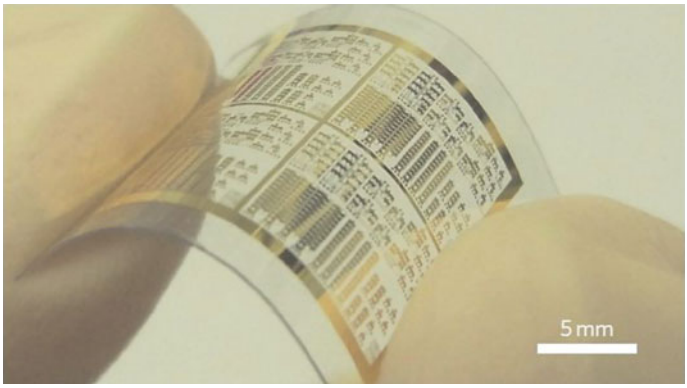

Fig. 23 Device fabrication on flexible and transparent PEN. (Reproduced with permission from ref [101]. © 2011, Macmillan Publisher Ltd)

purpose. Moreover, graphene with 2D nature provides distinctive advantages which are comparable with their fabrication methods. These exceptional advantages make graphene a favourable material for the stretchable or flexible electronics. The effective devices fabricated on a flexible and transparent PEN has been shown in Fig. 23.

4.2 Solar Energy Harvesting and Photocatalysis

There are two major challenges regarding the development of energy harvesting methods and protection of the environment. The possible solution is the conversion of solar energy into fuel or the electricity. For the best utilization of solar energy, three major processes containing ordered charge separation, maximum absorption of photons and the constructive use of separated charges. This major issue regarding energy harvesting needs the use of remarkable procedures in different environmental conditions. Hence, recent researches contain designing devices to concentrate the solar energy along with the improved understanding of the photovoltaic modules. If we increase the intensity of solar light, the response of photovoltaic devices can be improved. Especially, the important fields in utilization of solar energy are production of H_2 by water splitting, the conversion and storage of CO_2 operated through solar energy, development of solar cells which are sensitized to dyes, photocatalytic treatment of gas and waste water and the application of nanostructured material [102].

Fig. 24 An optical image of an industry-grade coin-shaped graphene-based supercapacitor device (Reproduced with permission from ref [103]. © 2009, ACS)

4.3 Supercapacitors

Supercapacitors, also known as the ultracapacitors or the ECs (electrochemical capacitors) form a unique energy storage system possessing environment friendly properties along with its low cost. It contains the advantage of easy storage and release of energy with a higher rate than that attainable with other batteries that are used for the purpose of energy storage. The energy density of these supercapacitors is greater than traditional dielectric capacitors. They can balance the high demand of energy by replacement of batteries for energy harvesting application. Since 1957, when General Electric established the practical application of electrochemical capacitors for the purpose of energy storage, supercapacitors with large reliability and small load cycles are regarded to be ideal along with sources for energy recapturing by forklifts, electrical vehicles and the load cranes [103]. Figure 24 shows the optical image of a industry grade coin-shaped graphene-based supercapacitor device.

4.4 Photovoltaic and Photoelectrochemical Devices

The photovoltaic and the photoelectrochemical devices based on graphene and its composites have notable applications for optical and electronic properties for production of electricity. Though, pure graphene was firstly presented as the transparent electrode material as applications in solar cells and these are turned out as successful electrode material for applications in photovoltaic and also the photoelectrochemical devices [104]. Nanocomposites of graphene give possible conductive electrodes to the ITO (indium tin oxide) porous films and sheets of pure graphene in the photovoltaic cells along with photoelectrochemical devices [105]. In this regard, sulphur particles are incorporated in graphene to be used in Li-S batteries as illustrated in Fig. 25.

Fig. 25 Wrapped S-particles (in graphene) for their use in Li–S batteries (Reproduced with permission from ref [111]. © 2011, ACS)

4.5 Electrochemical Energy Devices

4.5.1 Li-ion Batteries and Li-Batteries

The electrode material for the Li-ion batteries is provided by graphene due to its slight weight, greater surface area and the high conductivity [106]. Nanocomposites of graphene contain remarkable potential for many applications like enhancing cycling stability, rate performance and the capacitance in the LIBs (lithium-ion batteries) [107–110]. The nanocomposites of graphene with S, Si, metal oxides and the complex compounds are used as electrodes in LIBs. Graphene presence improves the performance of LIBs like Li–S batteries [111]. Graphene based nanocomposites have a high specific capacity of 900 $mAhg^{1}$, great rate capability and cycling stability [108]. Graphene forms a porous structure along with a conductive pathway for easy diffusion of Li-ions. As formed hybrid film contains properties like high-rate capability along with cycling stability by having 496 mAg^{1} of specific capacity at about 100 mAg^{1} after about 40 cycles [109].

Beside of their use in Li-ion batteries, nanocomposites of graphene can also be directly used in LIBa or Li–S batteries [111–114]; and they have proven to be as excellent material for formation of cathode in rechargeable LIBs [111] (Fig. 25).

4.5.2 Na-ion Batteries

Recently, the Na-ion batteries has captivated interest researchers to use as energy storing devices due to its properties like inexpensive, environment friendly and most importantly its abundance on earth crust as it is 6th most copious element in earth crust [115–118]. As in Fig. 26 by applying charge and discharge current, there occurs back and forth movement of Na^{+} between cathode and anode [119]. The ionic flow is managed by electronic movement from the circuit. Many materials can be used for the formation of electrode in Na-ion batteries like hard carbon, graphitic carbon, alloys of Na like P, Sn, Sb and Sn etc. along with some of the conversion materials like transition metal sulfide and oxide as the anode material and pyrophosphates, layered oxides and polyanionic phosphates ad the cathode material [116–118]. The organic materials are proven to be best suitable for the Na-ion batteries along with environment friendliness [120]. However, researches are being made for the selection

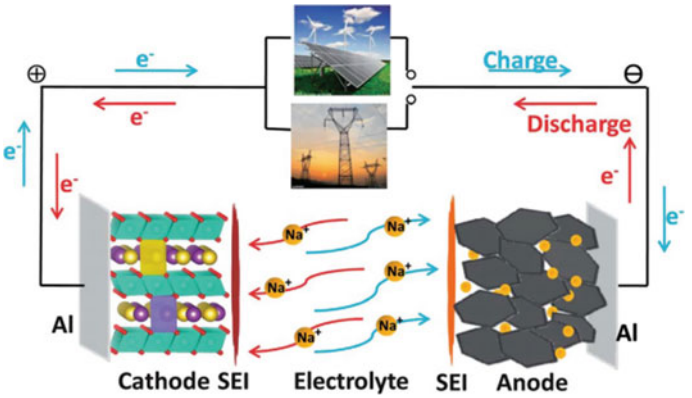

Fig. 26 Schematic diagram representing the Na-ion battery of rocking chair type with their working principle (Reproduced with permission from ref [119]. © 2013, RSC)

of suitable material in Na batteries. Due to the greater size of Na as compared to Li, limits the availability of the host materials [121].

4.5.3 Zn–Air Batteries

In the case of these batteries, the alkaline liquid electrolyte produces charge by mixing Zn with atmospheric O_2 (Fig. 27) [122]. The capacity of charge produced by Zn-air batteries is five times higher than Li-ion batteries. The capacity of charge produced by Zn-air batteries is five times higher than Li-ion batteries. Zn-air batteries are lighter, durable, safer and cheaper than that of Li-ion batteries with theoretical energy density of the order of 1086 $WhKg^{-1}$. Furthermore, many challenges are present in these batteries like formation of carbonates in air electrodes, small cell voltage as well as the slow-kinetic of the OER (oxygen evolution reaction) and ORR (oxygen reduction reaction). For the production of efficient and bifunctional batteries for OER and ORR processes, advanced researches are being done [123–127]. Nanosheets of graphene containing large surface area can present substrate for the growth of functional nanomaterials for the achievement of Zn-air batteries with high performance. In fact, there are advanced nanomaterials of graphene with bifunctional air-breathing cathode that perform efficient electrocatalytic activity that can reduce overpotential along with increase in cyclic stability of the rechargeable Zn-air batteries [128].

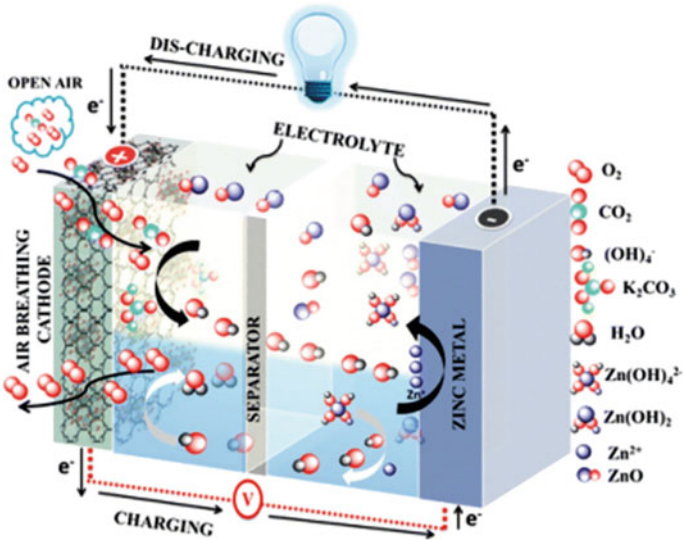

Fig. 27 Schematic diagram showing operation of the rechargeable aprotic Zn-air battery (Reproduced with permission from ref [122]. © 2014, ACS)

4.6 Photocatalytic Hydrogen Generation

Hydrogen is considered to be a type of clean and environment friendly fuel. By applying suitable photocatalyst, photocatalytic hydrogen evolution along with solar energy harvesting was regarded as a clean and efficient way for production of energy from hydrogen by using it as fuel [129, 130]. Many of the semiconductor photocatalysts are reported that are used for H_2 production from the H_2O [131, 132]. Many efforts are made for the utilization of nanocomposites of graphene for production of photocatalytic hydrogen. In this regard, activity of photocatalysts of graphene can be enhanced by incorporation with noble metals which are then used for production of photocatalytic hydrogen.

However, in early work, there was limited formation of H_2-pairs on sheets of graphite due to its hindered adsorption on graphite surface [133], photocatalysts based on graphene can produce photocatalytic hydrogen on their surface. This is possible because of the accumulation of photogenerated electrons on the graphene surface. Therefore, C-atoms present on graphene sheets can reduce H^+ to H_2 by the use of electrons produced during photocatalytic reaction. For the production of H_2 from water, graphite oxide is proven to be the best catalyst because of the presence of suitable levels for oxidation to occur [132].

5 Summary and Outlook

There is increasing energy demands due to the increasing population of the world due to increased power consumption which is predicted to become double in coming few decades. Hence, there is a need for researchers and scientists to advance clean, sustainable and renewable energy technology, they can meet the growing challenges and demands of energy economically and should be environment friendly. [134–138]. The extensive use of the carbon fuels and their unfortunate environmental effects pushed this world in a paragon where there is need for the application of green methods and systems. Many of the environmental issues including acid rain and global warming are due to the unmediated response of excessive use of fossil fuels. The nanocomposites are based on graphene containing appreciable growth in the technology due to its applications. The use of H_2 as energy source is favourable due to its negligible release to the environment [126, 139, 140]. Along with many other materials, 2D carbon containing graphene is regarded as favourable material for storage of hydrogen because of its properties like lightweight, chemical stability, large surface area and the pronounced onboard reversibility [141].

For the production of the photocatalytic hydrogen, the photocatalysts based on graphene are demonstrated as favourable photocatalytic materials. In this regard, many researches have worked to prove the use of photocatalytic graphene-based materials for designing the procedure to produce photocatalytic H_2. Presence of graphene has proven to be important in these materials for hydrogen production [129]. The effectiveness of the multicomponent photocatalysts based on graphene in the photocatalytic reactions is proven to be effective by recent results [131]. The effective charge distribution in different energy levels in multicomponent nanocomposites can be facilitated by adjusting band gap in energy levels of constituent materials. Significant improvement in photocatalysis can be achieved by optimal selection of shape, size and the composition of the multicomponent nanocomposites based on graphene. For designing and developing the photocatalytic material containing high performance, the best solution is the effective transfer of electron between the interface. Efforts are being made for the development of controlled and cost-effective methods to fabricate the 3D framework and its transformation along with development of the graphene doped with heteroatoms for the practical applications [142].

However, there are few challenges to be managed in order to manifest the capability of nanocomposites based on graphene regarding its applications, cost and synthetic methods. One of the main challenges is production of graphene and its composites on a large scale, which comprises enormous effects. Some of the challenges present are: (i) how we can prevent the formation of graphene clusters in matrix, (ii) how we can control most defects on the surface; and (iii) how we can tune application-based characteristics. Anyhow, there are many techniques to produce graphene, although few methods have been reported for commercialization of the energy storage appliances of graphene. To address these challenges, new methods and setups are needed for improvement of performance and properties of the graphene [143].

Their applications as fuel-cell batteries, supercapacitors and catalysts have been acknowledged with great exception during past few decades [136–138]. Certainly, the utilization of graphene-based composites in above mentioned applications is a new attempt presenting that research efforts in future will be profound. One challenge is the maintenance of the outstanding physical properties of the graphene for the synthesis of the nanocomposites [28]. One prediction is the development of elementary route via direct oxidation method of graphene by soft templating method for production of little bit functionalities as to furnish active sites of graphene with the nanoparticles. One important characteristic is that it has no need for composite reduction due to its lower oxidation condition, producing graphene framework with lesser defects [144].

The development in the field of hybrids and nanocomposites of graphene is notable. However, significant work is to be done in the field where they show applications as electrochemical devices and catalysts [145]. However, new probabilities are opened for utilization and better understanding of the graphene to overcome the knowledge gap [146]. Still, for the understanding of the fundamental application of the composites, significant attention is still needed.

References

1. Lee, C.-G., Park, S., Ruoff, R.S., Dodabalapur, A.: Integration of reduced graphene oxide into organic field-effect transistors as conducting electrodes and as a metal modification layer. Appl. Phys. Lett. **95**(2), 188 (2009)
2. Liao, K.-H., Kobayashi, S., Kim, H., Abdala, A.A., Macosko, C.W.: Influence of functionalized graphene sheets on modulus and glass transition of PMMA. Macromolecules **47**(21), 7674–7676 (2014)
3. Guo, C.X., Yang, H.B., Sheng, Z.M., Lu, Z.S., Song, Q.L., Li, C.M.: Layered graphene/quantum dots for photovoltaic devices. Angew. Chem. Int. Ed. **49**(17), 3014–3017 (2010)
4. Pletikosić, I., et al.: Dirac cones and minigaps for graphene on Ir (111). Phys. Rev. Lett. **102**(5), 056808 (2009)
5. Tang, L., Wang, Y., Li, Y., Feng, H., Lu, J., Li, J.: Preparation, structure and electrochemical properties of graphene modified electrode. Adv. Funct. Mater. **19**, 2782–2789 (2009)
6. Du, X., Skachko, I., Barker, A., Andrei, E.Y.: Approaching ballistic transport in suspended graphene. Nat. Nanotechnol. **3**(8), 491–495 (2008)
7. Huang, X., et al.: Graphene-based materials: synthesis, characterization, properties, and applications. Small **7**(14), 1876–1902 (2011)
8. Zhu, Y., et al.: Graphene and graphene oxide: synthesis, properties, and applications. Adv. Mater. **22**(35), 3906–3924 (2010)
9. Stankovich, S., et al.: Graphene-based composite materials. Nature **442**(7100), 282–286 (2006)
10. Novoselov, K.S., Geim, A.: The rise of graphene. Nat. Mater. **6**(3), 183–191 (2007)
11. Xu, C., Wang, X., Zhu, J.: Graphene− metal particle nanocomposites. J. Phys. Chem. C **112**(50), 19841–19845 (2008)
12. Geim, A.K., Novoselov, K.S.: The rise of graphene. Nat. Mater. **6**, 183–191 (2007)
13. Kim, H., Abdala, A.A., Macosko, C.W.: Graphene/polymer nanocomposites. Macromolecules **43**(16), 6515–6530 (2010)

14. Wu, S., Yin, Z., He, Q., Lu, G., Zhou, X., Zhang, H.: Electrochemical deposition of Cl-doped n-type Cu 2 O on reduced graphene oxide electrodes. J. Mater. Chem. **21**(10), 3467–3470 (2011)
15. Schwierz, F.: Graphene transistors. Nat. Nanotechnol. **5**(7), 487 (2010)
16. Verdejo, R., Bernal, M.M., Romasanta, L.J., Lopez-Manchado, M.A.: Graphene filled polymer nanocomposites. J. Mater. Chem. **21**(10), 3301–3310 (2011)
17. Bortz, D.R., Heras, E.G., Martin-Gullon, I.: Impressive fatigue life and fracture toughness improvements in graphene oxide/epoxy composites. Macromolecules **45**(1), 238–245 (2012)
18. Yin, Z., et al.: Electrochemical deposition of ZnO nanorods on transparent reduced graphene oxide electrodes for hybrid solar cells. Small **6**(2), 307–312 (2010)
19. Shen, J., Shi, M., Yan, B., Ma, H., Li, N., Ye, M.: One-pot hydrothermal synthesis of Ag-reduced graphene oxide composite with ionic liquid. J. Mater. Chem. **21**(21), 7795–7801 (2011)
20. Shi, Y., et al.: Graphene wrapped LiFePO 4/C composites as cathode materials for Li-ion batteries with enhanced rate capability. J. Mater. Chem. **22**(32), 16465–16470 (2012)
21. Zhang, H., Lv, X., Li, Y., Wang, Y., Li, J.: P25-graphene composite as a high performance photocatalyst. ACS Nano **4**(1), 380–386 (2010)
22. Novoselov, K., Mishchenko, A., Carvalho, A., Neto, A.C.: 2D materials and van der Waals heterostructures. Science **353**(6298), aac9439 (2016)
23. Cao, A., et al.: A facile one-step method to produce graphene–CdS quantum dot nanocomposites as promising optoelectronic materials. Adv. Mater. **22**(1), 103–106 (2010)
24. Zhang, W., et al.: A strategy for producing pure single-layer graphene sheets based on a confined self-assembly approach. Angew. Chem. **121**(32), 5978–5982 (2009)
25. López, V., et al.: Chemical vapor deposition repair of graphene oxide: a route to highly-conductive graphene monolayers. Adv. Mater. **21**(46), 4683–4686 (2009)
26. Li, D., Müller, M.B., Gilje, S., Kaner, R.B., Wallace, G.G.: Processable aqueous dispersions of graphene nanosheets. Nat. Nanotechnol. **3**(2), 101–105 (2008)
27. Xu, C., Wang, X., Zhu, J., Yang, X., Lu, L.: Deposition of Co 3 O 4 nanoparticles onto exfoliated graphite oxide sheets. J. Mater. Chem. **18**(46), 5625–5629 (2008)
28. Boukhvalov, D.W., Katsnelson, M.I.: Modeling of graphite oxide. J. Am. Chem. Soc. **130**(32), 10697–10701 (2008)
29. Verma, D., Goh, K.L.: Functionalized graphene-based nanocomposites for energy applications. In: Functionalized Graphene Nanocomposites and their Derivatives, pp. 219–243. Elsevier (2019)
30. Niu, L., Coleman, J.N., Zhang, H., Shin, H., Chhowalla, M., Zheng, Z.: Production of two-dimensional nanomaterials via liquid-based direct exfoliation. Small **12**(3), 272–293 (2016)
31. Ciesielski, A., Samori, P.: Graphene via sonication assisted liquid-phase exfoliation. Chem. Soc. Rev. **43**(1), 381–398 (2014)
32. Hernandez, Y., et al.: High-yield production of graphene by liquid-phase exfoliation of graphite. Nat. Nanotechnol. **3**(9), 563–568 (2008)
33. Raccichini, R., Varzi, A., Passerini, S., Scrosati, B.: The role of graphene for electrochemical energy storage. Nat. Mater. **14**(3), 271–279 (2015)
34. Abdelkader, A., Cooper, A., Dryfe, R., Kinloch, I.: How to get between the sheets: a review of recent works on the electrochemical exfoliation of graphene materials from bulk graphite. Nanoscale **7**(16), 6944–6956 (2015)
35. Ambrosi, A., Pumera, M.: Electrochemically exfoliated graphene and graphene oxide for energy storage and electrochemistry applications. Chem.–Eur. J. **22**(1), 153–159 (2016)
36. Yu, G., et al.: Solution-processed graphene/MnO_2 nanostructured textiles for high-performance electrochemical capacitors. Nano Lett. **11**(7), 2905–2911 (2011)
37. Lewandowska, M., Krawczyńska, A.T., Kulczyk, M., Kurzydłowski, K.J.: Structure and properties of nano-sized Eurofer 97 steel obtained by hydrostatic extrusion. J. Nucl. Mater. **386**, 499–502 (2009)
38. Bekyarova, E., et al.: Electronic properties of single-walled carbon nanotube networks. J. Am. Chem. Soc. **127**(16), 5990–5995 (2005)

39. Baskaran, D., Mays, J.W., Bratcher, M.S.: Noncovalent and nonspecific molecular interactions of polymers with multiwalled carbon nanotubes. Chem. Mater. **17**(13), 3389–3397 (2005)
40. Haghseresht, F., Finnerty, J., Nouri, S., Lu, G.: Adsorption of aromatic compounds onto activated carbons: effects of the orientation of the adsorbates. Langmuir **18**(16), 6193–6200 (2002)
41. Trang, L.K.H., Thanh Tung, T., Young Kim, T., Yang, W.S., Kim, H., Suh, K.S.: Preparation and characterization of graphene composites with conducting polymers. Polym. Int. **61**(1), 93–98 (2012)
42. Zhou, C., Szpunar, J.A., Cui, X.: Synthesis of Ni/graphene nanocomposite for hydrogen storage. ACS Appl. Mater. Interfaces **8**(24), 15232–15241 (2016)
43. Stankovich, S., et al.: Synthesis of graphene-based nanosheets via chemical reduction of exfoliated graphite oxide. Carbon **45**(7), 1558–1565 (2007)
44. Xu, Y., et al.: A graphene hybrid material covalently functionalized with porphyrin: synthesis and optical limiting property. Adv. Mater. **21**(12), 1275–1279 (2009)
45. Yang, H., Shan, C., Li, F., Han, D., Zhang, Q., Niu, L.: Covalent functionalization of polydisperse chemically-converted graphene sheets with amine-terminated ionic liquid. Chem. Commun. **26**, 3880–3882 (2009)
46. Putz, K.W., Compton, O.C., Segar, C., An, Z., Nguyen, S.T., Brinson, L.C.: Evolution of order during vacuum-assisted self-assembly of graphene oxide paper and associated polymer nanocomposites. ACS Nano **5**(8), 6601–6609 (2011)
47. Liu, L.-H., Lerner, M.M., Yan, M.: Derivitization of pristine graphene with well-defined chemical functionalities. Nano Lett. **10**(9), 3754–3756 (2010)
48. Si, Y., Samulski, E.T.: Synthesis of water soluble graphene. Nano Lett. **8**(6), 1679–1682 (2008)
49. Englert, et al.: Covalent bulk functionalization of graphene. Nat. Chem. **3**(4), 279–286 (2011)
50. Liu, L.-H., Yan, M.: Simple method for the covalent immobilization of graphene. Nano Lett. **9**(9), 3375–3378 (2009)
51. Fang, M., Wang, K., Lu, H., Yang, Y., Nutt, S.: Covalent polymer functionalization of graphene nanosheets and mechanical properties of composites. J. Mater. Chem. **19**(38), 7098–7105 (2009)
52. Fang, M., Wang, K., Lu, H., Yang, Y., Nutt, S.: Single-layer graphene nanosheets with controlled grafting of polymer chains. J. Mater. Chem. **20**(10), 1982–1992 (2010)
53. Chang, H., Wu, H.: Graphene-based nanocomposites: preparation, functionalization, and energy and environmental applications. Energy Environ. Sci. **6**(12), 3483–3507 (2013)
54. Moon, G.-h, Park, Y., Kim, W., Choi, W.: Photochemical loading of metal nanoparticles on reduced graphene oxide sheets using phosphotungstate. Carbon **49**(11), 3454–3462 (2011)
55. Ng, Y.H., Iwase, A., Bell, N.J., Kudo, A., Amal, R.: Semiconductor/reduced graphene oxide nanocomposites derived from photocatalytic reactions. Catal. Today **164**(1), 353–357 (2011)
56. Pasricha, R., et al.: Directed nanoparticle reduction on graphene. Mater. Today **15**(3), 118–125 (2012)
57. Zhang, Y., Yuan, X., Wang, Y., Chen, Y.: One-pot photochemical synthesis of graphene composites uniformly deposited with silver nanoparticles and their high catalytic activity towards the reduction of 2-nitroaniline. J. Mater. Chem. **22**(15), 7245–7251 (2012)
58. Tjoa, V., Chua, J., Pramana, S.S., Wei, J., Mhaisalkar, S.G., Mathews, N.: Facile photochemical synthesis of graphene-Pt nanoparticle composite for counter electrode in dye sensitized solar cell. ACS Appl. Mater. Interfaces **4**(7), 3447–3452 (2012)
59. Xu, F., Sun, Y., Zhang, Y., Shi, Y., Wen, Z., Li, Z.: Graphene–Pt nanocomposite for nonenzymatic detection of hydrogen peroxide with enhanced sensitivity. Electrochem. Commun. **13**(10), 1131–1134 (2011)
60. Chen, J., Zheng, X., Wang, H., Zheng, W.: Graphene oxide-Ag nanocomposite: In situ photochemical synthesis and application as a surface-enhanced Raman scattering substrate. Thin Solid Films **520**(1), 179–185 (2011)
61. Anandhan, S., Bandyopadhyay, S.: Polymer nanocomposites: from synthesis to applications. Nanocompos. Polym. Anal. Methods **1**, 1–28 (2011)

62. Akharame, M.O., Fatoki, O.S., Opeolu, B.O., Olorunfemi, D.I., Oputu, O.U.: Polymeric nanocomposites (PNCs) for wastewater remediation: an overview. Polym.-Plast. Technol. Eng. **57**(17), 1801–1827 (2018)
63. Caro, C.: UV/VIS Spectrophotometry–Fundamentals and Application. Mettler-Toledo Publication (2015)
64. Moecher, D.P.: Characterization and identification of mineral unknowns: a mineralogy term project. J. Geosci. Educ. **52**(1), 5–9 (2004)
65. Argast, A., Tennis, C.F., III.: A web resource for the study of alkali feldspars and perthitic textures using light microscopy, scanning electron microscopy and energy dispersive X-Ray spectroscopy. J. Geosci. Educ. **52**(3), 213–217 (2004)
66. Williams, D.B., Carter, C.B.: Transmission Electron Microscopy. Springer, Boston (1996)
67. Hirsch, P.B., Howie, A., Nicholson, R.B., Pashley, D.W., Whelan, M.J.: Electron microscopy of thin crystals. Phys. Today **19**(10), 3 (1966)
68. Wang, X., Chen, S.: Graphene-based nanocomposites. In: Physics and Applications of Graphene-Experiments, pp. 135–168 (2011)
69. Xu, C., Wang, X.: Fabrication of flexible metal-nanoparticle films using graphene oxide sheets as substrates. Small **5**(19), 2212–2217 (2009)
70. Dikin, D.A., et al.: Preparation and characterization of graphene oxide paper. Nature **448**(7152), 457–460 (2007)
71. Chong, S.W., Lai, C.W., Hamid, S.B.A.: Green preparation of reduced graphene oxide using a natural reducing agent. Ceram. Int. **41**(8), 9505–9513 (2015)
72. Baloyi, S., Ngqalakwezi, A., Nkazi, D., Ntho, T.: Investigation of graphene-based nanocomposite for hydrogen storage. IOP Conf. Ser. Mater. Sci. Eng. **655**, 012029 (2019)
73. Gardiner, D.J.: Introduction to Raman scattering. In: Practical Raman Spectroscopy, pp. 1–12. Springer, Heidelberg (1989)
74. Prusty, K., Barik, S., Swain, S.K.: A corelation between the graphene surface area, functional groups, defects, and porosity on the performance of the nanocomposites. In: Functionalized Graphene Nanocomposites and their Derivatives, pp. 265–283. Elsevier (2019)
75. Han, Y., Lu, Y.: Characterization and electrical properties of conductive polymer/colloidal graphite oxide nanocomposites. Compos. Sci. Technol. **69**(7–8), 1231–1237 (2009)
76. Xu, Y., et al.: A hybrid material of graphene and poly (3, 4-ethyldioxythiophene) with high conductivity, flexibility, and transparency. Nano Res. **2**(4), 343–348 (2009)
77. McAloney, R.A., Sinyor, M., Dudnik, V., Goh, M.C.: Atomic force microscopy studies of salt effects on polyelectrolyte multilayer film morphology. Langmuir **17**(21), 6655–6663 (2001)
78. Schütte, M., Kurth, D.G., Linford, M.R., Cölfen, H., Möhwald, H.: Metallosupramolecular thin polyelectrolyte films. Angew. Chem. Int. Ed. **37**(20), 2891–2893 (1998)
79. Cutler, C.A., Bouguettaya, M., Kang, T.-S., Reynolds, J.R.: Alkoxysulfonate-functionalized PEDOT polyelectrolyte multilayer films: electrochromic and hole transport materials. Macromolecules **38**(8), 3068–3074 (2005)
80. Andrade, J.D.: X-ray photoelectron spectroscopy (XPS). In: Surface and Interfacial Aspects of Biomedical Polymers, pp. 105–195. Springer, Boston (1985)
81. Paredes, J., Villar-Rodil, S., Martínez-Alonso, A., Tascon, J.: Graphene oxide dispersions in organic solvents. Langmuir **24**(19), 10560–10564 (2008)
82. Stankovich, S., Piner, R.D., Chen, X., Wu, N., Nguyen, S.T., Ruoff, R.S.: Stable aqueous dispersions of graphitic nanoplatelets via the reduction of exfoliated graphite oxide in the presence of poly (sodium 4-styrenesulfonate). J. Mater. Chem. **16**(2), 155–158 (2006)
83. Kalil, H., Maher, S., Bose, T., Bayachou, M.: Manganese oxide/hemin-functionalized graphene as a platform for peroxynitrite sensing. J. Electrochem. Soc. **165**(12), G3133 (2018)
84. Hummers, W.S., Jr., Offeman, R.E.: Preparation of graphitic oxide. J. Am. Chem. Soc. **80**(6), 1339–1339 (1958)
85. Elgrishi, N., Rountree, K.J., McCarthy, B.D., Rountree, E.S., Eisenhart, T.T., Dempsey, J.L.: A practical beginner's guide to cyclic voltammetry. J. Chem. Educ. **95**(2), 197–206 (2018)
86. Oprea, R., et al.: Peroxynitrite activity of hemin-functionalized reduced graphene oxide. Analyst **138**(15), 4345–4352 (2013)

87. Peteu, S.F., Bose, T., Bayachou, M.: Polymerized hemin as an electrocatalytic platform for peroxynitrite's oxidation and detection. Anal. Chim. Acta **780**, 81–88 (2013)
88. Gee, B.: André Marie Ampère (1775–1836). Phys. Educ. **5**(6), 359 (1970)
89. Yan-Hong, Y., Run-Cai, M., Jin-Tao, B., Xun, H.: Photoluminescence of multiwalled carbon nanotubes excited at different wavelengths. Chin. Phys. **15**(11), 2761 (2006)
90. Goumri, M., Lucas, B., Ratier, B., Baitoul, M.: Electrical and optical properties of reduced graphene oxide and multi-walled carbon nanotubes based nanocomposites: a comparative study. Opt. Mater. **60**, 105–113 (2016)
91. Chung, W.-J., Sena, M., Merzlyak, A., Lee, S.-W.: Phages as Tools for Functional Nanomaterials Development (2011)
92. Lee, Y.-M., Huang, C.-M., Chen, H.-W., Yang, H.-W.: Low temperature solution-processed ZnO nanorod arrays with application to liquid ethanol sensors. Sens. Actuators A Phys. **189**, 307–312 (2013)
93. Balasubramani, V., Sureshkumar, S., Rao, T.S., Sridhar, T.: Impedance spectroscopy-based reduced graphene oxide-incorporated ZnO composite sensor for H_2S investigations. ACS Omega **4**(6), 9976–9982 (2019)
94. Barik, S., Choudhary, R., Mahapatra, P.: Impedance spectroscopy study of Na 1/2 Sm 1/2 TiO 3 ceramic. Appl. Phys. A **88**(1), 217–222 (2007)
95. Idrees, M., Nadeem, M., Mehmood, M., Atif, M., Chae, K.H., Hassan, M.: Impedance spectroscopic investigation of delocalization effects of disorder induced by Ni doping in LaFeO3. J. Phys. D Appl. Phys. **44**(10), 105401 (2011)
96. Seitz, M., Hampton, F., Richmond, W.: Influence of chemisorbed oxygen on the AC electrical behaviour of polycrystalline ZnO. In: Additives and Interfaces in Electronic Ceramics Proc Special Conf held at Cincinnati 4–5 May 1982 Advances in Ceramics (1982)
97. Jang, S., et al.: Flexible, transparent single-walled carbon nanotube transistors with graphene electrodes. Nanotechnology **21**(42), 425201 (2010)
98. Klauk, H., Halik, M., Zschieschang, U., Eder, F., Schmid, G., Dehm, C.: Relationship between molecular structure and electrical performance of oligothiophene organic thin film transistors. Appl. Phys. Lett. **82**, 4175–4177 (2003)
99. Nomura, K., Ohta, H., Takagi, A., Kamiya, T., Hirano, M., Hosono, H.: Room-temperature fabrication of transparent flexible thin-film transistors using amorphous oxide semiconductors. Nature **432**(7016), 488–492 (2004)
100. Suo, Z., Ma, E., Gleskova, H., Wagner, S.: Mechanics of rollable and foldable film-on-foil electronics. Appl. Phys. Lett. **74**(8), 1177–1179 (1999)
101. Sun, D.-m, et al.: Flexible high-performance carbon nanotube integrated circuits. Nat. Nanotechnol. **6**(3), 156–161 (2011)
102. Tang, J., Dai, S., Darr, J.A.: Recent developments in solar energy harvesting and photocatalysis. Int. J. Photoenergy **2012**, 580746 (2012)
103. Wang, Y., et al.: Supercapacitor devices based on graphene materials. J. Phys. Chem. C **113**(30), 13103–13107 (2009)
104. Wu, J., Becerril, H.A., Bao, Z., Liu, Z., Chen, Y., Peumans, P.: Organic solar cells with solution-processed graphene transparent electrodes. Appl. Phys. Lett. **92**(26), 237 (2008)
105. Chang, H., Liu, Y., Zhang, H., Li, J.: Pyrenebutyrate-functionalized graphene/poly (3-octylthiophene) nanocomposites based photoelectrochemical cell. J. Electroanal. Chem. **656**(1–2), 269–273 (2011)
106. Li, X., et al.: Graphene-on-silicon Schottky junction solar cells. Adv. Mater. **22**(25), 2743–2748 (2010)
107. Hu, L.-H., Wu, F.-Y., Lin, C.-T., Khlobystov, A.N., Li, L.-J.: Graphene-modified LiFePO 4 cathode for lithium ion battery beyond theoretical capacity. Nat. Commun. **4**(1), 1–7 (2013)
108. Wang, H., et al.: Mn3O4− graphene hybrid as a high-capacity anode material for lithium ion batteries. J. Am. Chem. Soc. **132**(40), 13978–13980 (2010)
109. Yu, A., Park, H.W., Davies, A., Higgins, D.C., Chen, Z., Xiao, X.: Free-standing layer-by-layer hybrid thin film of graphene-MnO2 nanotube as anode for lithium ion batteries. J. Phys. Chem. Lett. **2**(15), 1855–1860 (2011)

110. Zhou, X., Wang, F., Zhu, Y., Liu, Z.: Graphene modified LiFePO 4 cathode materials for high power lithium ion batteries. J. Mater. Chem. **21**(10), 3353–3358 (2011)
111. Wang, H., et al.: Graphene-wrapped sulfur particles as a rechargeable lithium–sulfur battery cathode material with high capacity and cycling stability. Nano Lett. **11**(7), 2644–2647 (2011)
112. Cao, Y., et al.: Sandwich-type functionalized graphene sheet-sulfur nanocomposite for rechargeable lithium batteries. Phys. Chem. Chem. Phys. **13**(17), 7660–7665 (2011)
113. Ji, L., et al.: Graphene oxide as a sulfur immobilizer in high performance lithium/sulfur cells. J. Am. Chem. Soc. **133**(46), 18522–18525 (2011)
114. Wang, J.-Z., Lu, L., Choucair, M., Stride, J.A., Xu, X., Liu, H.-K.: Sulfur-graphene composite for rechargeable lithium batteries. J. Power Sources **196**(16), 7030–7034 (2011)
115. Ji, L., et al.: Controlling SEI formation on SnSb-porous carbon nanofibers for improved Na ion storage. Adv. Mater. **26**(18), 2901–2908 (2014)
116. Kim, S., Seo, D., Ma, X., Ceder, G., Kang, K.: Adv. Energy Mater. **2**, 710 (2013). b) MD Slater, D. Kim, E. Lee, CS Johnson. Adv Funct Mater 23:947 2012
117. Kim, S.W., Seo, D.H., Ma, X., Ceder, G., Kang, K.: Electrode materials for rechargeable sodium-ion batteries: potential alternatives to current lithium-ion batteries. Adv. Energy Mater. **2**(7), 710–721 (2012)
118. Yabuuchi, N., Kubota, K., Dahbi, M., Komaba, S.: Research development on sodium-ion batteries. Chem. Rev. **114**(23), 11636–11682 (2014)
119. Pan, H., Hu, Y.-S., Chen, L.: Room-temperature stationary sodium-ion batteries for large-scale electric energy storage. Energy Environ. Sci. **6**(8), 2338–2360 (2013)
120. Wang, L.P., Yu, L., Wang, X., Srinivasan, M., Xu, Z.J.: Recent developments in electrode materials for sodium-ion batteries. J. Mater. Chem. A **3**(18), 9353–9378 (2015)
121. Zhou, H., et al.: Outstanding hydrogen evolution reaction catalyzed by porous nickel diselenide electrocatalysts. Energy Environ. Sci. **10**(6), 1487–1492 (2017)
122. Prabu, M., Ramakrishnan, P., Nara, H., Momma, T., Osaka, T., Shanmugam, S.: Zinc–air battery: understanding the structure and morphology changes of graphene-supported CoMn2O4 bifunctional catalysts under practical rechargeable conditions. ACS Appl. Mater. Interfaces **6**(19), 16545–16555 (2014)
123. Lee, D.U., Choi, J.Y., Feng, K., Park, H.W., Chen, Z.: Advanced extremely durable 3D bifunctional air electrodes for rechargeable zinc-air batteries. Adv. Energy Mater. **4**(6), 1301389 (2014)
124. Lee, J.S., et al.: Metal–air batteries with high energy density: Li–air versus Zn–air. Adv. Energy Mater. **1**(1), 34–50 (2011)
125. Li, L., Manthiram, A.: Long-life, high-voltage acidic Zn–air batteries. Adv. Energy Mater. **6**(5), 1502054 (2016)
126. Li, Y., Dai, H.: Recent advances in zinc–air batteries. Chem. Soc. Rev. **43**(15), 5257–5275 (2014)
127. Xu, Y., Zhang, Y., Guo, Z., Ren, J., Wang, Y., Peng, H.: Flexible, stretchable, and rechargeable fiber-shaped zinc–air battery based on cross-stacked carbon nanotube sheets. Angew. Chem. **127**(51), 15610–15614 (2015)
128. Wang, K., et al.: Dendrite growth in the recharging process of zinc–air batteries. J. Mater. Chem. A **3**(45), 22648–22655 (2015)
129. Li, Q., et al.: Highly efficient visible-light-driven photocatalytic hydrogen production of CdS-cluster-decorated graphene nanosheets. J. Am. Chem. Soc. **133**(28), 10878–10884 (2011)
130. Maeda, K., Domen, K.: Photocatalytic water splitting: recent progress and future challenges. J. Phys. Chem. Lett. **1**(18), 2655–2661 (2010)
131. Xiang, Q., Yu, J., Jaroniec, M.: Enhanced photocatalytic H 2-production activity of graphene-modified titania nanosheets. Nanoscale **3**(9), 3670–3678 (2011)
132. Zhang, J., Yu, J., Zhang, Y., Li, Q., Gong, J.R.: Visible light photocatalytic H2-production activity of CuS/ZnS porous nanosheets based on photoinduced interfacial charge transfer. Nano Lett. **11**(11), 4774–4779 (2011)
133. Casolo, S., Løvvik, O.M., Martinazzo, R., Tantardini, G.F.: Understanding adsorption of hydrogen atoms on graphene. J. Chem. Phys. **130**(5), 054704 (2009)

134. Chu, S., Majumdar, A.: Opportunities and challenges for a sustainable energy future. Nature **488**(7411), 294–303 (2012)
135. Dunn, B., Kamath, H., Tarascon, J.-M.: Electrical energy storage for the grid: a battery of choices. Science **334**(6058), 928–935 (2011)
136. Larcher, D., Tarascon, J.-M.: Towards greener and more sustainable batteries for electrical energy storage. Nat. Chem. **7**(1), 19–29 (2015)
137. Tarascon, J.-M., Armand, M.: Issues and challenges facing rechargeable lithium batteries. Nature **414**, 359–367 (2001)
138. Xu, K.: Electrolytes and interphases in Li-ion batteries and beyond. Chem. Rev. **114**(23), 11503–11618 (2014)
139. Schlapbach, L., Züttel, A.: Hydrogen-storage materials for mobile applications. Nature **414**, 353–358 (2001)
140. Wagemans, R.W., van Lenthe, J.H., de Jongh, P.E., Van Dillen, A.J., de Jong, K.P.: Hydrogen storage in magnesium clusters: quantum chemical study. J. Am. Chem. Soc. **127**(47), 16675–16680 (2005)
141. Chen, M.-L., Park, C.-Y., Choi, J.-G., Oh, W.-C.: Synthesis and characterization of metal (Pt, Pd and Fe)-graphene composites. J. Korean Ceram. Soc. **48**(2), 147 (2011)
142. Kumar, N.A., Baek, J.-B.: Doped graphene supercapacitors. Nanotechnology **26**(49), 492001 (2015)
143. Lightcap, I.V., Kamat, P.V.: Graphitic design: prospects of graphene-based nanocomposites for solar energy conversion, storage, and sensing. Acc. Chem. Res. **46**(10), 2235–2243 (2013)
144. Terrones, M., et al.: Interphases in graphene polymer-based nanocomposites: achievements and challenges. Adv. Mater. **23**(44), 5302–5310 (2011)
145. Chen, S., Zhu, J., Wang, X.: One-step synthesis of graphene− cobalt hydroxide nanocomposites and their electrochemical properties. J. Phys. Chem. C **114**(27), 11829–11834 (2010)
146. Zhou, M., et al.: Highly conductive porous graphene/ceramic composites for heat transfer and thermal energy storage. Adv. Func. Mater. **23**(18), 2263–2269 (2013)